



Natural Resources  
Canada

Ressources naturelles  
Canada

## **GEOLOGICAL SURVEY OF CANADA**

### **OPEN FILE 8706**

# **The ups and downs of the Canadian Shield: 3 – additional apatite fission-track analyses from the Musselwhite, Roberto, Meadowbank and Raglan mines, Ontario, Quebec, and Nunavut**

**N. Pinet and K. McDannell**

**2020**

**Canada**



## GEOLOGICAL SURVEY OF CANADA

### OPEN FILE 8706

# The ups and downs of the Canadian Shield: 3 – additional apatite fission-track analyses from the Musselwhite, Roberto, Meadowbank and Raglan mines, Ontario, Quebec, and Nunavut

N. Pinet<sup>1</sup> and K. McDannell<sup>2</sup>

<sup>1</sup>Geological Survey of Canada, 490, rue de la Couronne, Québec, Quebec G1K 9A9

<sup>2</sup>Geological Survey of Canada, 3303 33<sup>rd</sup> Street Northwest, Calgary, Alberta T2L 2A7

2020

© Her Majesty the Queen in Right of Canada, as represented by the Minister of Natural Resources, 2020  
Information contained in this publication or product may be reproduced, in part or in whole, and by any means, for personal or public non-commercial purposes, without charge or further permission, unless otherwise specified.

You are asked to:

- exercise due diligence in ensuring the accuracy of the materials reproduced;
- indicate the complete title of the materials reproduced, and the name of the author organization; and
- indicate that the reproduction is a copy of an official work that is published by Natural Resources Canada (NRCan) and that the reproduction has not been produced in affiliation with, or with the endorsement of, NRCan.

Commercial reproduction and distribution is prohibited except with written permission from NRCan. For more information, contact NRCan at [nrcan.copyrightdroitdauteur.rncan@canada.ca](mailto:nrcan.copyrightdroitdauteur.rncan@canada.ca).

Permanent link: <https://doi.org/10.4095/321845>

This publication is available for free download through GEOSCAN (<https://geoscan.nrcan.gc.ca/>).

#### Recommended citation

Pinet, N., and McDannell, K., 2020. The ups and downs of the Canadian Shield: 3 – additional apatite fission-track analyses from the Musselwhite, Roberto, Meadowbank and Raglan mines, Ontario, Quebec, and Nunavut; Geological Survey of Canada, Open File 8706, 51 p. <https://doi.org/10.4095/321845>

Publications in this series have not been edited; they are released as submitted by the author.

# The ups and downs of the Canadian Shield: 3– Additional apatite fission-track analyses from the Musselwhite, Roberto, Meadowbank and Raglan mines

Nicolas Pinet <sup>(1)</sup> and Kalin McDannell <sup>(2)</sup>

<sup>(1)</sup> Natural Resources Canada, Geological Survey of Canada, 490 rue de la Couronne, Québec, Quebec, G1K 9A9

<sup>(2)</sup> Natural Resources Canada, Geological Survey of Canada, 3303 33 St. NW, Calgary, AB, T2L 2A7

**Abstract:** The low-temperature ( $\text{ca}$  120–60°C) thermal history of nine samples from four mines was investigated using the apatite fission-track (AFT) method. Analyses correspond to four samples from the Musselwhite mine over a 275 m vertical interval, three from the Roberto mine over a 382 m vertical interval and one sample from both the Meadowbank and Raglan mines. AFT inverse modelling using both HeFTy and QTQt softwares yield concordant results and indicate that a Phanerozoic heating episode was minor (< 20°C) or non-existent over the Musselwhite mine. This contrasts with previous AFT studies that document significant heating (> 20°C) due to sedimentary burial and indicates that the Canadian Shield did not react as a single entity during the last billion years. The thermal history of samples from the Roberto and Meadowbank mines are less constrained due to the lack of ‘high’ (> 120°C) temperature constraints. The sample from the Raglan mine yields the youngest central age among the samples reported in this study.

## 1. Introduction

Cratons formed of Archean to Proterozoic age rocks survived multiple tectonic cycles and testify to a relative stability over periods of hundreds of million years, a behaviour related to some of the characteristics of the cratonic lithosphere (high thickness and stiffness, low temperature). However, the ‘stability paradigm’ may mask the complexity in the post-orogenic evolution of cratons. The tools available to study the dynamics of cratons over tens of millions to billions of years are fragmentary and yield, at best, an incomplete picture of their evolution. The sedimentary record preserved in intracratonic basins and platforms constrain the early subsidence history but the late stages of sediment deposition is generally poorly known as a significant portion of the succession may have been removed by erosion. Xenoliths and magmatism may provide some hints on the evolution of cratons but their significance at the craton scale is difficult to determine. Most geophysical observations, including seismic tomography, provide present-day snapshots, but they must be interpreted with caution when integrated in evolution models over time frames characteristic of cratons. Numerical models are increasingly used to discuss craton stability, but their results need to be tested against independent datasets.

Apatite fission-track (AFT) analysis is a well-established thermochronological method that constrains the thermal history at relatively low-temperatures (typically  $< 120^{\circ}\text{C}$ ). Despite the strong theoretical and methodological backgrounds of the AFT method, its application to relatively stable continental interiors presents some challenges. This is the case of the Canadian Shield which is characterized by slow exhumation rates during the Phanerozoic, low geothermal gradients and an incomplete geological record.

Here we report AFT data for nine samples from the Musselwhite, Roberto, Meadowbank and Raglan mines (Fig. 1) and provide preliminary interpretations. These datasets complement AFT analyses from the Hudson Bay regions reported in Pinet et al. (2016), Pinet (2018) and McDannell et al. (in press). This open file also aims to discuss modeling strategies and scenarios in more detail than it is usually possible in scientific journals and to make the

data (including single grain analysis, track length measurements and apatite geochemistry) available.

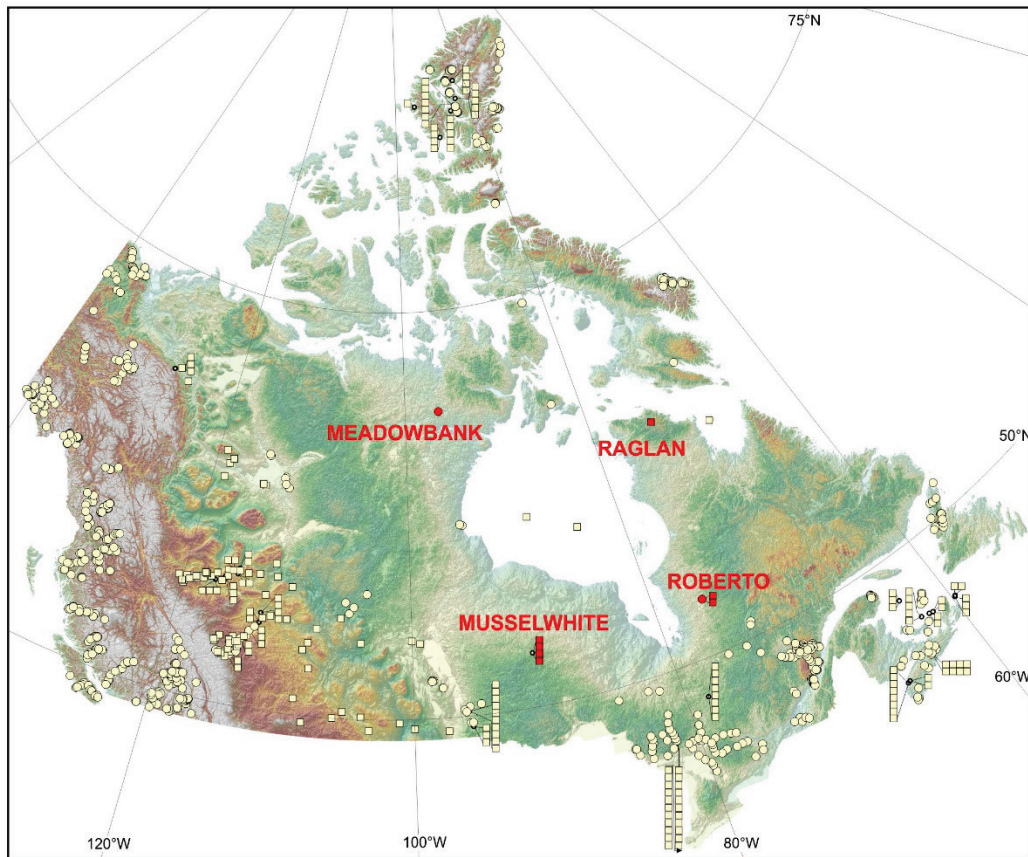


*Figure 1: Location of the Musselwhite, Roberto, Meadowbank and Raglan mines. Pale yellow circles (surface samples) and squares (drill hole/mine samples) correspond to available AFT analyses compiled by Pinet and Brake (2018).*

## 2. The apatite fission-track method

Apatite fission-track (AFT) analysis has been widely used during the past decades to constrain the low-temperature thermal histories of many areas around the world, in different geological settings. Isotopic dating methods are based on the ratio of parent and daughter isotopes, although for AFT analysis the daughter product is not another isotope but rather a trail of physical damage to the crystal lattice resulting from spontaneous fission of  $^{238}\text{U}$ .

Fission-tracks form at similar initial lengths continuously over time, at a rate dependent upon only uranium concentration. The fission-tracks are shortened in the partial annealing zone (PAZ) that corresponds to temperatures between ~60°C and ~120°C (>200°C for the most ‘retentive’ apatite). At temperatures lower than the PAZ, fission-tracks are still shortened but at much lower rates, whereas at higher temperatures, tracks are completely erased (annealed). During exhumation, earlier-formed tracks will tend to be shorter than later-formed ones, as they will have more time to anneal and may have experienced higher temperatures. The change in length of AFT varies among apatite crystals and two proxies are commonly used to estimate the kinetics of the annealing process: D<sub>par</sub>, the arithmetic mean of fission-track etch pit lengths measured parallel to the crystallographic c-axis (in µm; Burtner et al., 1994) and the chlorine content (in weight %; Green et al., 1985). In this study we prefer to use the kinetic parameter  $r_{mro}$  which characterizes the annealing behavior of apatite based on the multi-compositional calculation proposed by Carlson et al. (1999).

Interpretation of AFT data is based on the combined analysis of the fission-track age, track length distribution and a kinetic parameter. Fission-track ages do not usually indicate the timing of cooling through a specific temperature (except for nearly instantaneous cooling, such as in volcanic settings), but instead represent the integrated thermal history of studied samples. Excellent reviews on the AFT method are found in Gallagher et al. (1998), Gleadow et al. (2002), Donelick et al. (2005), Ketcham (2005) Green and Duddy (2012) and in the recent textbook dedicated to fission-track thermochronology and its application to geology (Malusà and Fitzgerald, 2019).

In this study we report inverse modelling results using two popular thermal history modelling programs: HeFTy (Ketcham, 2005 and 2013) and QTQt (Gallagher, 2012). These programs use the same physical principles but different inverse modelling approaches (see Vermeesch and Tian, 2014, Gallagher and Ketcham, 2018 and McDannell et al., in press for a review and discussion). HeFTy employs a non-directed random Monte Carlo search algorithm and each time-temperature path is compared to measured values using p-value thresholds as goodness-of-fit objective function criteria for both AFT ages and track length distribution. In QTQt, the inversion scheme implements a Bayesian reversible jump Markov chain Monte Carlo

(MCMC) routine in which time-temperature points are iteratively sampled to construct and refine a continuous thermal history by linear interpolation between sampled points that provide the best fit to the observed data. The Bayesian approach naturally prefers simpler thermal history models (which provide an adequate fit to the observations) rather than more complex histories (that may/may not provide better fits). Multiple samples with constant geometrical relationships through time (as a vertical profile) can be modelled together in QTQt.

### 3. AFT dataset

The AFT analyses reported here were conducted at Dalhousie University (Canada) using the external detector method. All rock samples were broken into small pieces using a hydraulic splitter and jaw crusher, then ground in a disc mill and sieved to fragments <500 µm. The sieved material was then run over a Wifley mineral separation table to produce an initial heavy mineral concentrate, which was then treated with conventional magnetic and heavy liquid techniques to produce an apatite-bearing fraction. Apatite aliquots were mounted in araldite epoxy on glass slides, ground and polished to an optical finish to expose internal grain surfaces. Polished mounts were etched in 5M HNO<sub>3</sub> for 20 seconds at 21°C to reveal the fossil tracks that intersect the polished apatite grain surface.

In the external detector method, the <sup>238</sup>U parent concentration is determined by using fission-track density induced on a uranium free external detector (muscovite slab) from the fission of <sup>235</sup>U through irradiation with a flux of slow thermal neutrons (see Donelick et al., 2005 for details). Samples and CN5 glass standards were irradiated with thermal neutrons. After irradiation, the low-U muscovite detectors that covered apatite grain mounts and glass dosimeter were etched in 5.5 M HNO<sub>3</sub> for 20 s at 21°C to reveal induced fission-tracks.

Results for the 9 samples analyzed are summarized on Table 1. It should be noted that parameters required for the zeta calibration (zeta and uncertainty in zeta, specific to each analyst) vary among the samples (Table 1).

Sample No	Lithology	Age	Mine	Location	Longitude	Latitude	Depth or elevation (m)	Nb of mounts	$\rho_s \times 10^6 \text{ cm}^3$	$\rho_i \times 10^6 \text{ cm}^3$	$\rho_d \times 10^6 \text{ cm}^3$	$P(X^2)$	Central Age $\pm$	U (ppm)	Confined track lengths	MTL ( $\mu\text{m} \pm$ STD)	Dpars ( $\mu\text{m}$ )	
							(m)		(Ni)	(Nd)			$1\sigma (\text{Ma})$					
<b>2016 DATASET</b>																		
MW12-UG-105	Iron formation	PK	Musselwhite Mine	Level 1770- section 11780	-90.36633	52.61159	-770	1	20	2.632 (910)	1.180 (408)	1.26 (5269)	81.8	490.49 $\pm$ 31.79	12.15	11	11.12 $\pm$ 0.57	2.9
MW12-UG-023	Iron formation	PK	Musselwhite Mine	level 1220-section 12150	-90.36633	52.61159	-920	1	22	1.651 (915)	0.697 (386)	1.23 (5269)	99.8	507.23 $\pm$ 33.39	7.51	11	11.84 $\pm$ 0.85	2.47
MW13-UG-010	Iron formation	PK	Musselwhite Mine	level 1020 - section 1230	-90.36633	52.61159	-1020	1	21	2.251 (1629)	1.060 (767)	1.27 (5269)	36.3	471.48 $\pm$ 25.04	13.72	85	11.77 $\pm$ 0.24	2.66
MW13-UG-018	Iron formation	PK	Musselwhite Mine	level 1045- section 12890	-90.36633	52.61159	-1045	1	19	2.291 (1882)	1.022 (840)	1.28 (5269)	46.9	507.92 $\pm$ 29.88	9.11	18	11.83 $\pm$ 0.59	2.53
RAGLAN 2	gabbro	PK	Raglan Mine	Zone 5-9; hole 718-3403	-73.67725	61.6876	-630	1	27	0.271 (127)	0.224 (105)	1.31 (5269)	47.2	280.82 $\pm$ 37.73	2.3	1	14.1	2.34
<b>2017 DATASET</b>																		
EOC-14-005	greywacke	PK	Roberto Mine	DEC_ROBERTO	-76.08658	52.69931	220.0	3	12	1.0460(681)	0.7004(456)	1.2064 (4351)	49.6	325.50 $\pm$ 20.77	9	6	12.21 $\pm$ 1.15	2.36
EUG-15-018A	greywacke	PK	Roberto Mine	Mine level 230	-76.08679	52.70057	-5.0	3	12	4.0473(527)	2.2502(293)	1.2171 (4351)	54.70	393.40 $\pm$ 29.76	25	128	12.49 $\pm$ 0.85	2.4
EUG-14-20C	greywacke	PK	Roberto Mine	Mine level 380_AMN357	-76.08623	52.70091	-162.0	3	24	0.9466(550)	0.6299(366)	1.1956 (4351)	33.2	324.62 $\pm$ 22.87	7	24	11.92 $\pm$ 2.59	2.28
MBK-12-493	diorite	PK	Meadowbank Mine	Open pit	-96.07229	65.02244		3	29	0.5300(1185)	0.25885(578)	1.2204 (4351)	99.2	447.73 $\pm$ 24.46	27	32	12.27 $\pm$ 1.64	2.42
<b>2016 AND 2017 DATASETS</b>																		
Zeta		362.7	2016 DATASET		370.6													
Zeta error		7.8			5													
ND		5269			4351													
Decay k																		
RhoD																		
Area																		
Ns																		
ps																		
Ni																		
pi																		
Nd																		
pd																		
MTL																		
X <sup>2</sup> test																		
Dpar																		
U																		
PK																		

Decay k  
RhoD  
Area  
Ns  
ps  
Ni  
pi  
Nd  
pd  
MTL  
X<sup>2</sup> test  
Dpar  
U  
PK

( $P > 2\%$ ) is a pass on the  $\chi^2$  test  
four Dpar measurements were averaged from each analysed crystal when available;  
when several track lengths were taken in the same grain, four Dpar measurements were made too. The Dpar values are the mean of those 4 Dpar values.  
average U concentration (ppm) of grains used for age calculation  
Precambrian

Table 1: Summary of AFT results

#### 4. Inverse Modeling- Musselwhite Mine

##### 4a- AFT Results

The Musselwhite mine is a gold deposit hosted in a polydeformed amphibolite facies banded iron-formation of the Mesoarchean North Caribou greenstone belt, northwestern Superior province (Fig. 1; Oswald et al., 2015). The four samples analyzed belong to a strongly folded chert-grunerite ± magnetite facies iron formation (Fig. 2A).

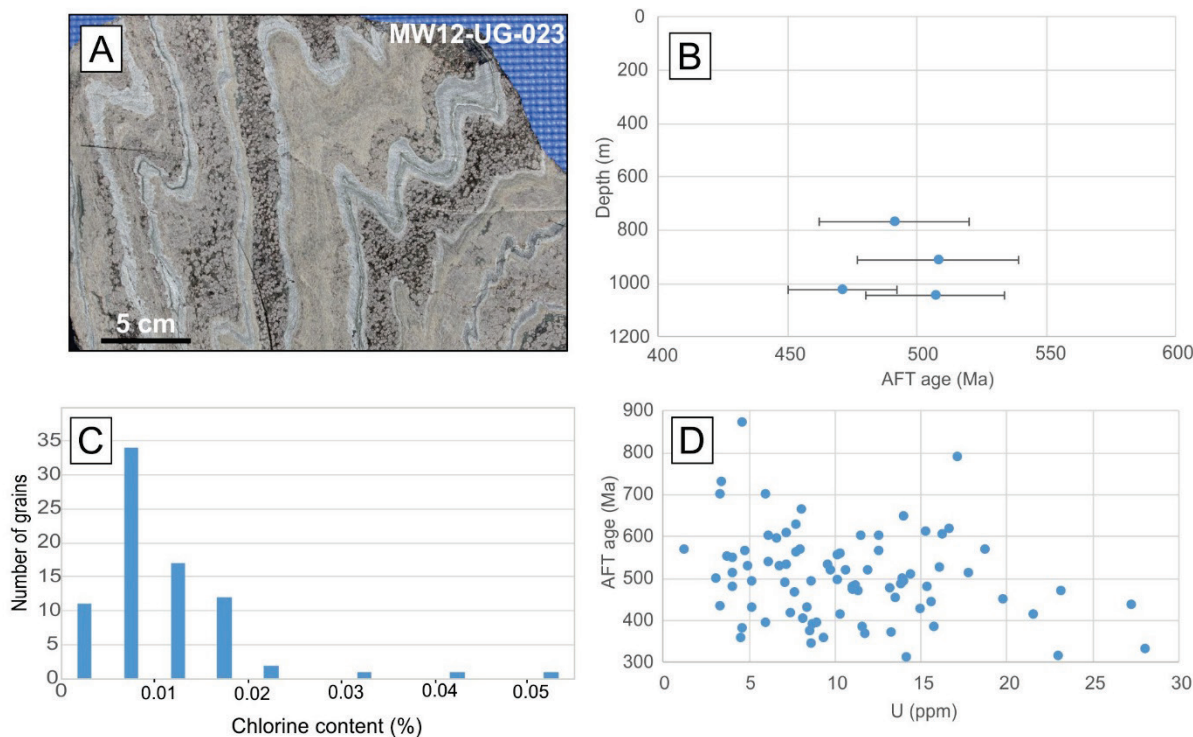


Figure 2: Musselwhite Mine. A) Deformed chert-grunerite iron formation. Sample MW12-UG-023; B) AFT Age versus depth diagram; C) Chlorine content of apatite grains from the four samples; D) Uranium content versus single-grain AFT age for the four samples.

Samples from the Musselwhite mine were collected over a vertical interval of 275 m at depths between 770 m and 1045 m. For each sample, the age determination is based on 19 to 22 apatite grains and track length data include between 11 and 85 measurements. AFT ages are within age uncertainties and varies between  $471.5 \pm 25.0$  and  $507.9 \pm 29.9$  Ma. The expected relationship between AFT age and elevation (with the deepest sample expected to

yield the youngest age) is not documented, probably due to the relatively short vertical interval (Fig. 2B).

Electron microprobe analyses of apatites indicate near end-member fluorapatite, with Chlorine content (Cl wt%) ranging from 0.002 to 0.051% (Fig. 2C; average = 0.012%). Apatite grains with such low values of Cl wt% usually anneal more readily relative to those with higher Cl wt% (> 1-2%), (Donelick et al., 2005). No clear relationship exists between etch pit diameter (Dpar) and Cl content/rmr0.

AFT ages tend to decrease with increasing single grain Uranium content (Fig. 2D). A similar relationship has been documented by McDannell et al. (2019a) for several samples from the Canadian Shield and interpreted as related to  $\alpha$ -radiation enhanced fission-track annealing, a mechanism that may be significant in slowly-cooled terranes.

#### 4b- Basic HeFTy model – sample MW13-UG-010

Among the four samples, sample MW13-UG-010 shows the lowest AFT age uncertainty and, more importantly, the greatest number of measured track lengths. It is thus considered as the most ‘robust’ sample and will be used as the reference sample for modelling.

Sample MW13-UG-010 yielded a central AFT age of  $471.5 \pm 25.0$  Ma. Oldest and youngest single grain ages are  $668.2 -210/+298$  and  $370.5 -102/+138$  Ma respectively (Fig. 3A).

The mean track length (non-projected) is  $11.77 \pm 0.24$   $\mu\text{m}$ . C-axis projected horizontal track lengths range between 10.69 and 16.54  $\mu\text{m}$  and show an unimodal distribution.

All apatite grains analysed are compositionally homogeneous with chlorine content  $\leq 0.03\%$ . Mean Dpar values (average of four measurements by crystals when available) average  $2.66 \mu\text{m}$ . No relationship exists between AFT age and Chlorine content or Dpar suggesting that the annealing kinetics of single grains in the sample are homogeneous.

The basic inverse model includes only two constraints: 1) a temperature of  $180 \pm 20^\circ\text{C}$  at  $975 \pm 25$  Ma based on the  $^{40}\text{Ar}/^{39}\text{Ar}$  results from a sample located at approximately 40 km (McDannell et al., 2018); 2) a present-day temperature of  $23 \pm 5^\circ\text{C}$  (depth = 1020 m). The time-temperature paths between 1 Ga and present-day include 25 segments, are qualified as ‘intermediate’ (no sudden changes) and are characterized by cooling rates  $< 2^\circ\text{C}$  (typical of cratonic settings). Inverse modelling stops when 50 good paths have been found.

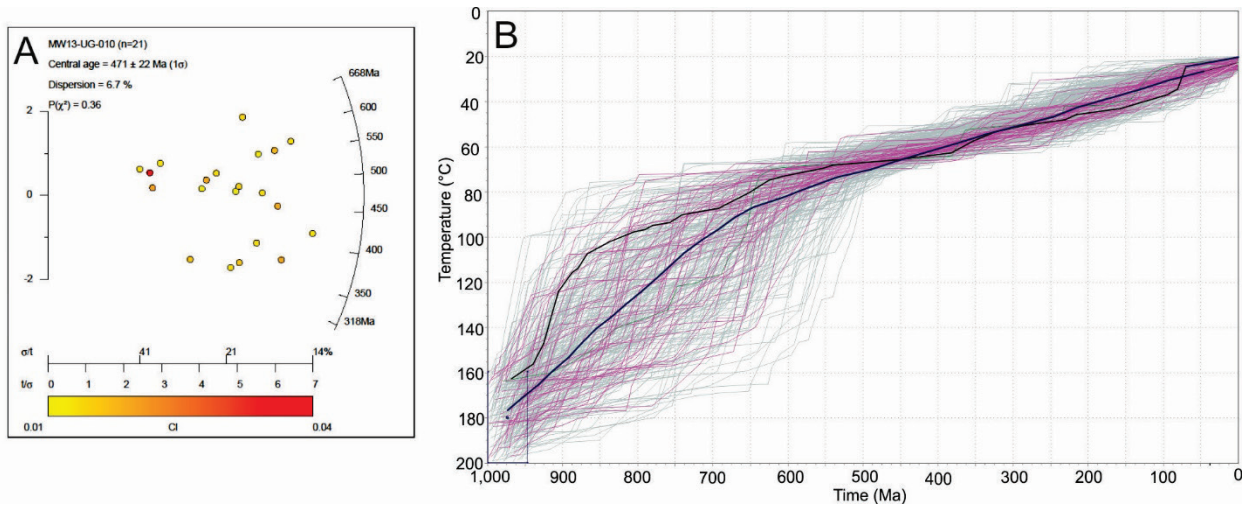


*Figure 3: Sample MW13-UG-010. A) Radial plot; On this diagram, more precise fission track ages plot further from the origin along the x-axis (precision). Data plotted using Radial Plotter software (Vermeesch, 2009). B) Inverse model results with the ‘basic’ scenario; The best fit path is shown in dark blue and the weighted mean path in black.*

Modeling results indicate that both the AFT age (goodness of fit = 0.92), track length distribution (goodness of fit = 0.99) and oldest predicted single grain age (673 Ma) can be adequately fit with a continuous cooling with rates decreasing at ca 600 Ma (Fig. 3B).

#### 4c- HeFTy model – composite sample MW13-UG-010+MW13-UG-018+MW12-UG-023

The low number of measured track lengths in three samples (MW13-UG-010, MW13-UG-018 and MW12-UG-023) add significant uncertainty to inverse models. Rather than model these samples, we combined the three samples located at 920 to 1045 m depth in a single composite sample (Fig. 4A; 62 apatite grains; 114 measured fission-tracks). The present-day

difference in temperature between these sample is less than 2° C and is not expected to play a significant role during inverse modelling.

The basic model includes the same two constraints as sample MW13-UG-010 (see section 4b above). Modeling results indicate that both the AFT age (goodness of fit = 0.93) and the track length distribution (goodness of fit = 0.87) can be adequately fit with a nearly monotonic cooling (Fig. 4B).

The number of grains is high enough to investigate the potential role of grain chemistry. In the case of the Musselwhite composite sample, Cl is the best parameter to distinguish two populations (Fig. 4C), even if it should be noted that both are close to the fluorapatite end-member. Distinguishing these populations in the basic model does not significantly modify the results (Fig. 4D).

An alternative model aims to ‘force’ some increase in temperature during the Paleozoic (Figs 4E and 4F). This scenario is a working hypothesis aiming to test an alternative thermal history and, indirectly, provide a qualitative evaluation of the basic model. In the ‘forced’ heating model, a time-temperature constraint is defined at 450 Ma (the age of the base of the sedimentary succession regionally) with temperatures  $\pm 30^{\circ}\text{C}$  the weighted mean path of the basic model. A loosely defined period of increase in temperature (potentially linked with subsidence) is imposed between 445 and 350 Ma. The timeframe (Late Ordovician-Early Devonian) corresponds to the most probable period for initial sedimentary burial (if any) based on regional considerations (Pinet et al., 2013; Lavoie et al., 2015). Modelling results indicate that AFT age (goodness of fit = 0.92) and track length distribution (goodness of fit = 1.00) can also be fit with this scenario. Both the best fit path and the weighted mean path show only moderate increase in temperature in the 445-350 Ma time interval ( $<8^{\circ}\text{ C}$  in both cases), even if higher temperatures were ‘allowed’ by the model. In other words, results from the ‘forced’ heating scenario are only slightly different from the basic model and indicate that the increase in temperature during the Paleozoic, if any, was minor.

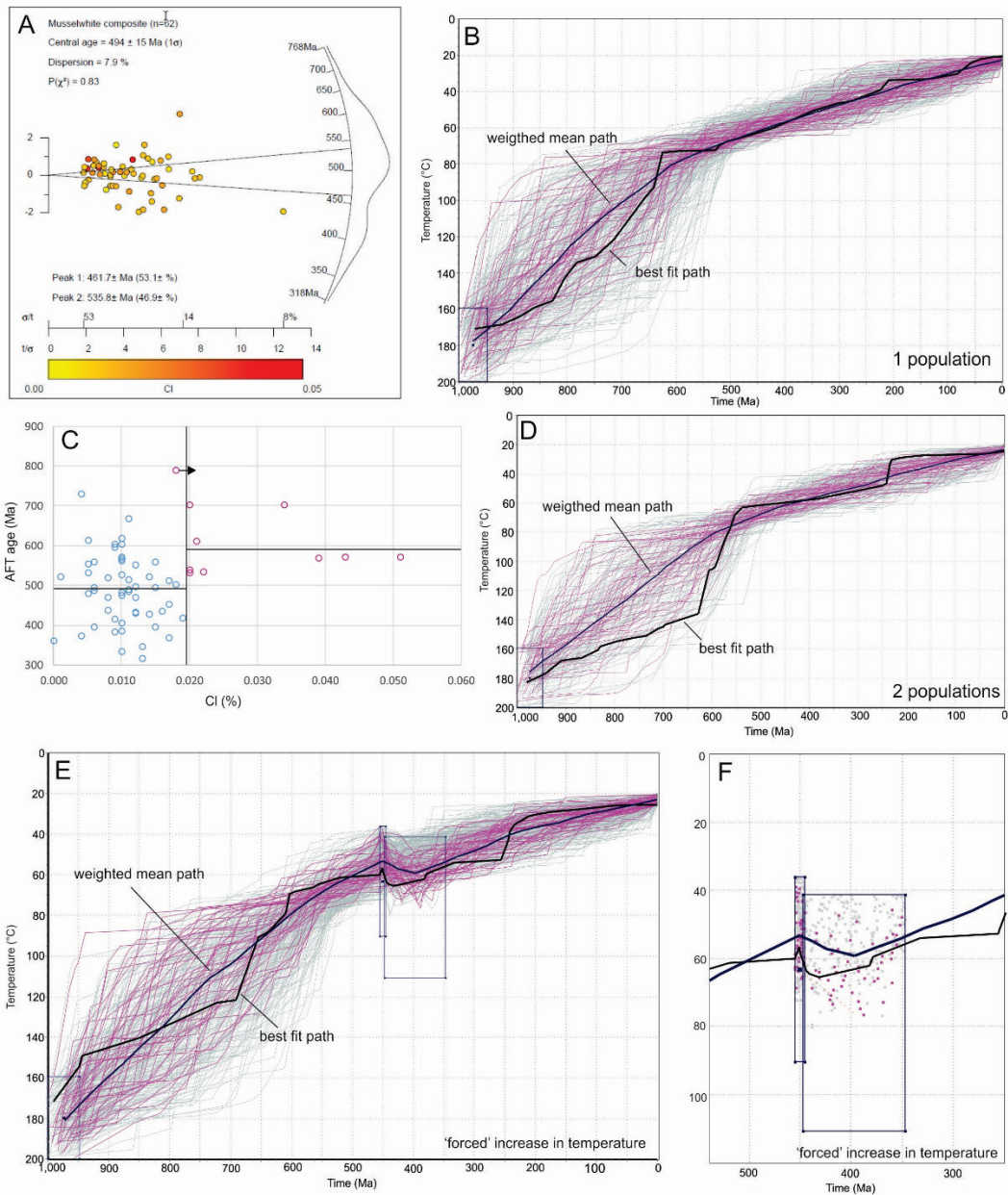


**Figure 4:** Composite sample MW12-UG-010 + MW-UG-018 + MW12-UG-023. A) Radial plot; On this diagram, more precise fission-track ages plot further from the origin along the x-axis (precision). Data plotted using Radial Plotter software (Vermeesch, 2009). B) Inverse model results with the 'basic' scenario; C) CI versus AFT age diagram used for distinguishing apatite populations; D) Inverse model results with the 'basic' scenario and two apatite populations. E) and F) Inverse model results with the scenario 'imposing' an heating episode during the Paleozoic. In B), D) and E) Good and acceptable paths are in magenta and grey respectively. The best fit path is shown in dark blue and the weighted mean path in black. In F) peak heating points within each of the T-t constrain boxes are indicated in magenta (good fits) and grey (acceptable fits)

#### 4d - QTQt model – vertical profile

AFT results from the four Musselwhite mine samples have been kept separate and modeled as a vertical profile using the QTQt software. The temperature constraint at 1000-950 Ma is the same as the HeFTy models. Maximum heating/cooling rates were fixed at 5°C. The model was run for over 300,000 iterations and showed good convergence.

The expected model (the preferred single model, a weighted mean model where the weighting is provided by the posterior probability) indicates that a continuous cooling accounts for the data (Fig. 5). This expected model shows a significant decrease in cooling rates at ~ 550 Ma, in close agreement with HeFTy models. The 95% credible intervals reflects the uncertainty of the model and indicate that the possibility of a slight increase in temperature between 480 and 350 Ma (green arrow on Fig. 5) cannot be ruled out. This time interval includes the period of sedimentation recorded in the Hudson Bay Basin.

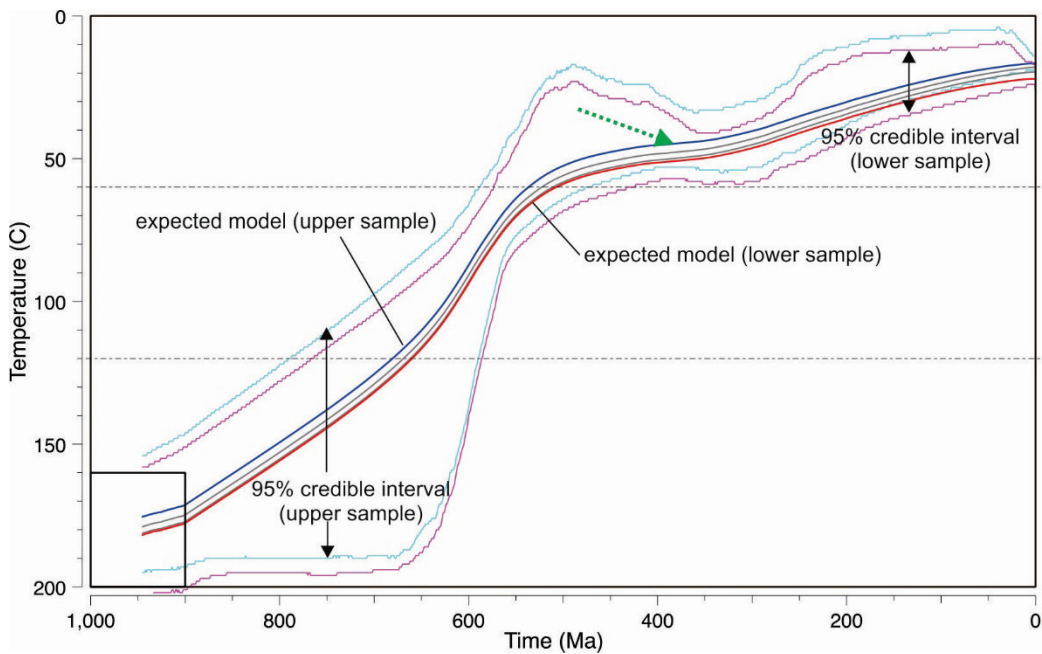


Figure 5: QTQt inverse modeling results for the four samples from the Musselwhite Mine. The green dotted arrow illustrate a possible slight increase in temperature during the Paleozoic.

## **5. Inverse modelling, Roberto mine**

### 5a- AFT results

The Roberto mine is a gold deposit hosted in polydeformed upper-greenschist to amphibolite facies metagreywacke (Low Formation) in the La Grande subprovince close to the contact with the amphibolite to granulite-facies Opinaca subprovince (Fontaine et al., 2015). The three samples analyzed are fine- to coarse grained deformed greywackes (Figs. 6A and 6B)

Samples from the Roberto mine were collected over a vertical interval of 382 m from surface (220 m) to a depth of 162 m. For each sample, the age determination is based on 12 to 24 apatite grains and track length data include between 6 and 128 measurements. AFT central ages vary between  $324.6 \pm 22.9$  and  $393.4 \pm 29.8$  Ma, thus ages are significantly younger than those from the Musselwhite mine. The expected relationship between the AFT age and the elevation (with the deepest sample expected to yield the youngest age) is not documented, probably due to the relatively short vertical interval.

Electron microprobe analyses of apatites indicate near end-member fluorapatite, with Chlorine content (Cl wt%) ranging from 0.000 to 0.019% (Fig. 6C; average = 0.005%). Apatite grains with such low values of Cl wt% usually anneal more readily relative to those with higher Cl wt% (> 1-2%), (Donelick et al., 2005). No clear relationship exists between etch pits diameter (Dpar) and Chlorine content.

Contrary to the Musselwhite Mine, there is no clear decrease of AFT ages with increasing single grain Uranium content (Fig. 6D).

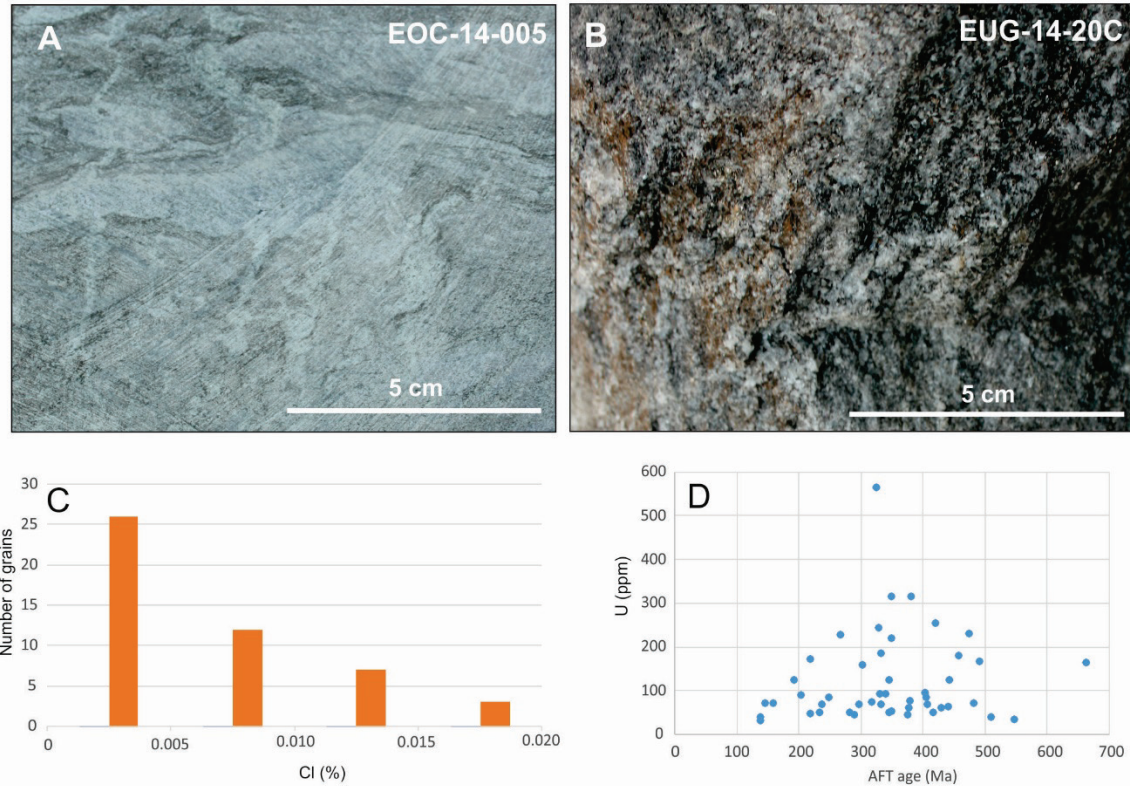


*Figure 6: Roberto mine. A) and B) fine- and coarse-grained greywackes. Samples EOC-14-005 and EUG-14-20C; C) Chlorine content of apatite grains from the three samples; D) Uranium content versus single-grain AFT age for the three samples.*

#### 5b- HeFTy models

None of the three samples from the Roberto Mine have enough single grain age data AND measured fission-track lengths to be adequately modelled. To overcome this issue, we combined the sample with the highest number of apatite grain (N=24; EUG-14-20C) with the sample with the highest number of measured tracks (N= 128; EUG-14-018A) in a single composite sample (Fig. 7A). These samples are located at 5 and 162 m depth and the present-day difference in temperature between these sample is less than 3° C which is not expected to play a significant role during inverse modelling. Oldest and youngest single grain ages are 666.6 and 138.2 Ma respectively.

The basic inverse model includes only two constraints: 1) due to the lack of data documenting the thermal history below the AFT partial annealing zone ( $> 120^{\circ}\text{C}$ ), the temperature is loosely constrained ( $160 \pm 40^{\circ}\text{C}$ ) at  $975 \pm 25$  Ma; 2) a present-day temperature of  $10 \pm 4^{\circ}\text{C}$ . The time-temperature paths between 1 Ga and present include 25 segments, are qualified as ‘intermediate’ (no sudden changes) and are characterized by cooling rates  $< 2^{\circ}\text{C}$  (typical of cratonic settings).

Modeling results indicate that both the AFT age (goodness of fit = 0.96) and the track length distribution (goodness of fit = 0.98) can be adequately fit with a nearly monotonic cooling (Fig. 7B). An alternative model (not shown) aims to ‘force’ some decrease in temperature during the Paleozoic using the same approach as the Musselwhite example (temperature constraint at 450 Ma =  $\pm 30^{\circ}\text{C}$  the weighted mean path of the basic model and a loosely defined period of increase in temperature between 445 and 350 Ma). Both the best-fit path and the weighted mean path of the ‘forced heating’ model do not show any significant increase in temperature in the 445–350 Ma time interval.

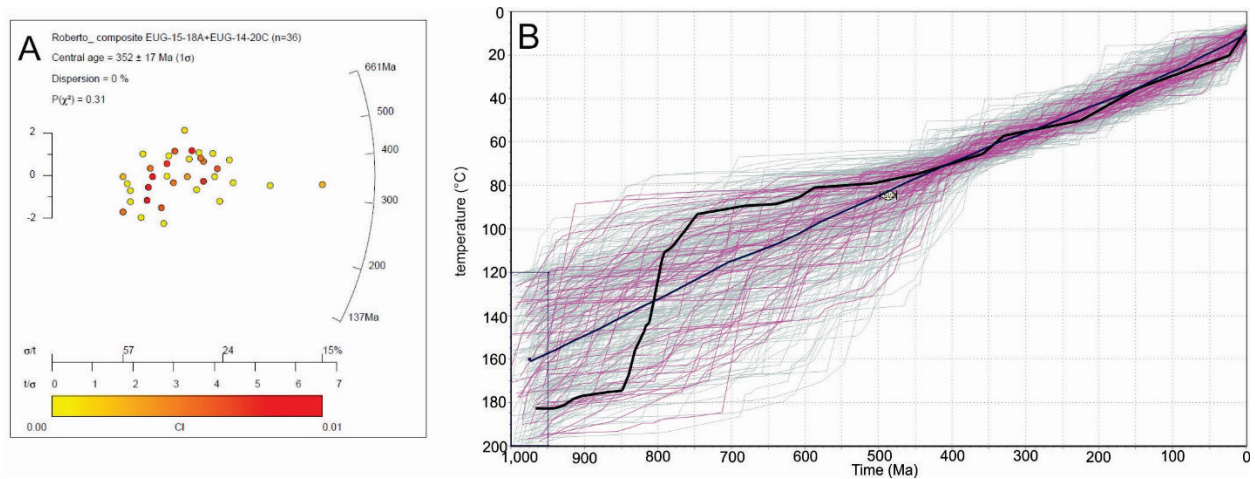


*Figure 7: Roberto mine composite sample. A) Radial plot; On this diagram, more precise fission-track ages plot further from the origin along the x-axis (precision). Data plotted using Radial Plotter software (Vermeesch, 2009). B) Inverse model results with the ‘basic’ scenario; The best fit path is shown in dark blue and the weighted mean path in black.*

Results from both the ‘basic’ and ‘forced heating’ models are however unable to explain the fact that some apatite grains have been partially annealed. Also in both cases, the predicted oldest single grain ages are < 475 Ma, significantly lower than measured (666.6 Ma). In order to account for partial annealing, we test a scenario in which samples were located relatively close to surface (35 < temperature < 70°C) at ca 500 Ma. Inverse modeling results (Fig. 8) show good fits for age and length (0.97 and 0.94 respectively) and an oldest predicted single grain age of 624 Ma. In this model, both the best-fit path and the weighted mean path show moderate (20-30°C) temperature increase during the Paleozoic.

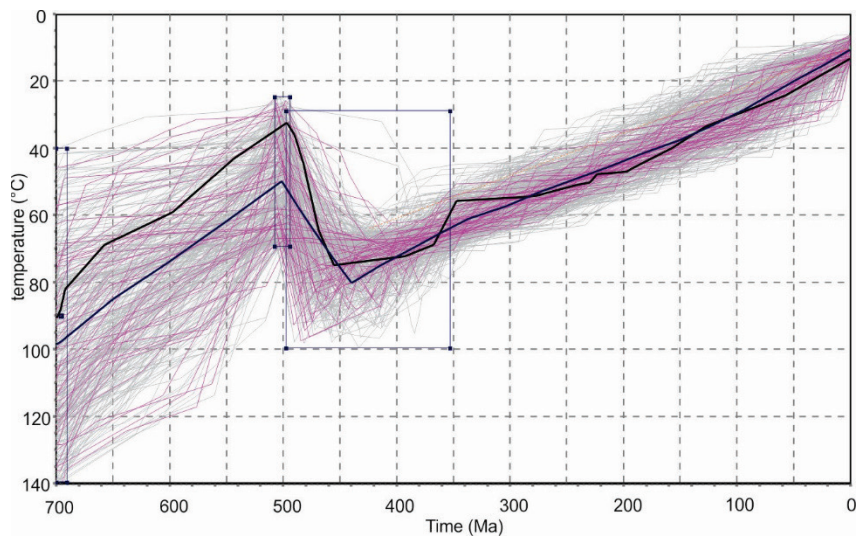


*Figure 8: Inverse model results with the scenario in which samples were located relatively close to surface (35 < temperature < 70°C) at ca 500 Ma. Good and acceptable paths are in magenta and grey respectively. The best fit path is shown in dark blue and the weighted mean path in black.*

### 5c- QTQt model – vertical profile

AFT results from the three Roberto mine samples have been kept separate and modeled as a vertical profile in QTQt software. Maximum heating/cooling rates were fixed at 5°C. The model was run for over 300,000 iterations and showed good convergence.

The expected model (the preferred single model, a weighted mean model where the weighting is provided by the posterior probability) indicates that a continuous cooling accounts

for the data (Fig. 9). However, the 95% credible interval reflects the uncertainty of the model and that there is a possibility of a significant ( $> 20^{\circ}\text{C}$ ) increase in temperature during the Paleozoic (green arrow on Fig. 9).

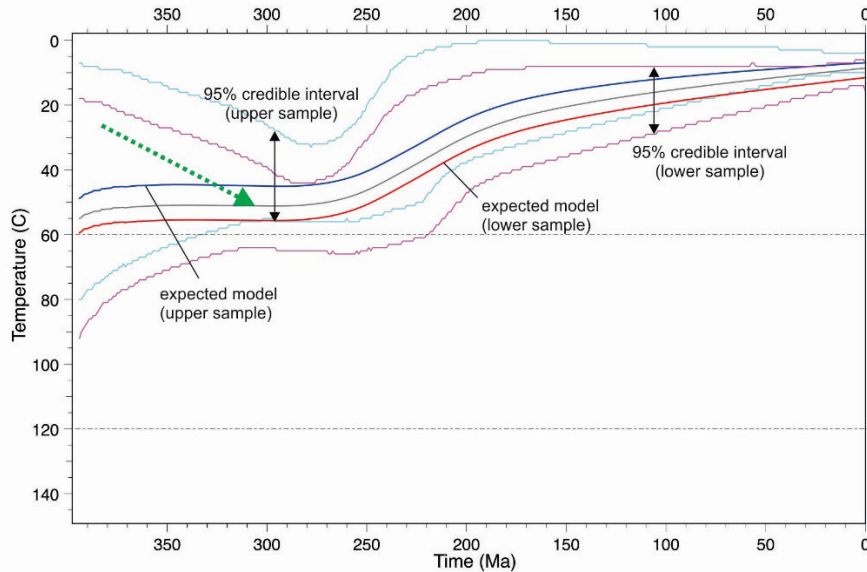


*Figure 9: QTQt inverse modeling results for the three samples from the Roberto mine.*

## 6. Meadowbank Mine

The Meadowbank gold deposit (Nunavut) is hosted in greenschist- to amphibolite-grade polydeformed Neoarchean banded iron formation within the Rae domain of the western Churchill Province (Janvier et al., 2015).

Sample MBK-12-493 yielded a central AFT age of  $447.7 \pm 24.5$  Ma, based on 29 apatite grains. (Fig. 10A). The mean track length (non-projected) is  $12.27 \pm 1.64$   $\mu\text{m}$ . All apatite grains analysed are compositionally homogeneous with chlorine content  $< 0.1\%$ . AFT ages decrease with increasing single grain Uranium content (Fig. 10B).

The basic inverse model includes the same constraints as for the Roberto mine (two T-t constraints only). Results suggest a nearly monotonic cooling (Fig. 10C; goodness of fit of 0.77 and 0.88 for AFT age and track length respectively). The model with a ‘forced’ increase in

temperature during the Paleozoic (not shown) shows a very low increase in temperature in the 445-350 Ma time interval ( $\pm 4^{\circ}\text{C}$  for the weighted mean path;  $\pm 0^{\circ}\text{C}$  for the best fit path). A model (not shown) with relatively low ( $35 < t < 70^{\circ}\text{C}$ ) temperatures at *ca* 500 Ma (similar to the one tested for the Roberto mine) yields comparable results.

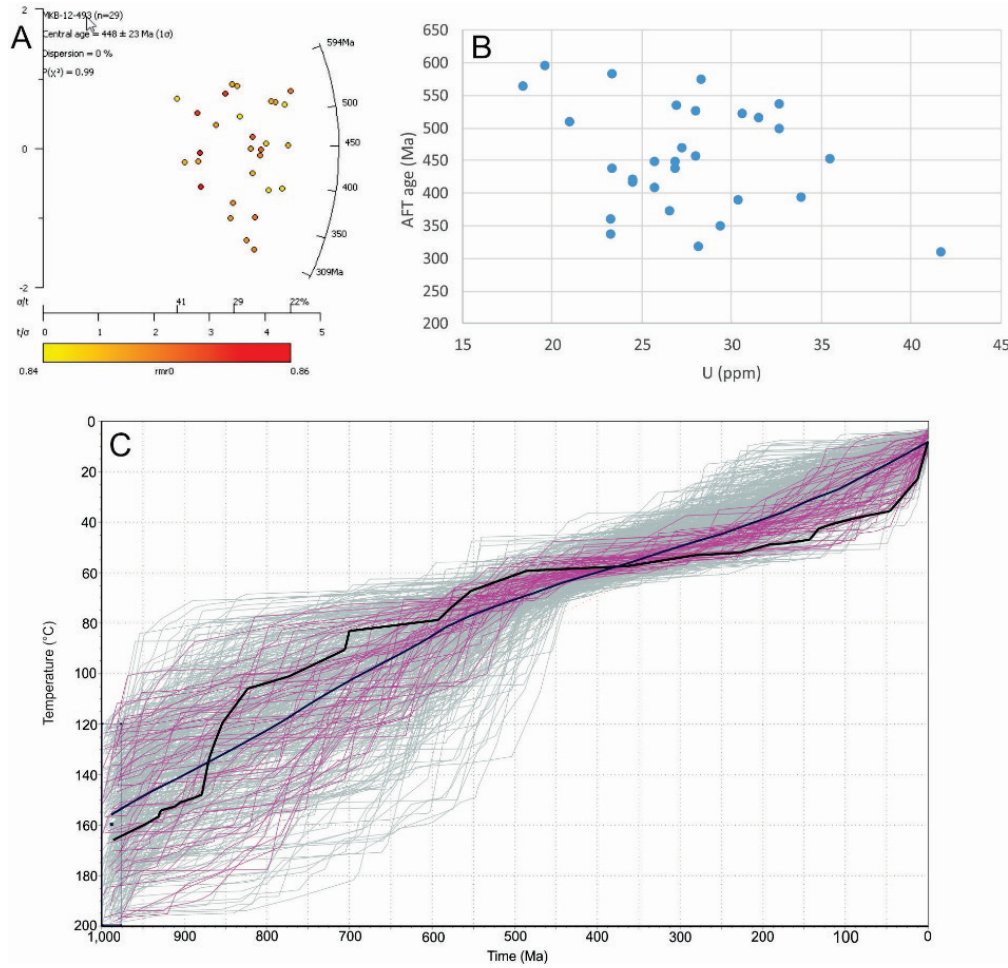


*Figure 10: Meadowbank mine sample. A) Radial plot; On this diagram, more precise fission-track ages plot further from the origin along the x-axis (precision). Radial plot done using the Radial Plotter software (Vermeesch, 2009). B) Uranium content versus AFT age diagram; C) Inverse model results with the 'basic' scenario; The best fit path is shown in dark blue and the weighted mean path in black.*

## 7. Raglan Mine

The Raglan Mine (Quebec) is a Nickel-Cu-(PGE) deposit hosted with a series of mafic-ultramafic complexes in the lower greenschist facies of the east-central part of the early Proterozoic Cape Smith Belt of the Ungava Peninsula (Lesher, 2007). Four samples

corresponding to the rock types distinguished by mine geologists ('normal' gabbro, mafic gabbro, sediments and volcanics) with weight > 10 kg were collected in the Raglan mine. Only one gabbroic sample located at a depth of 630 m yielded enough apatite grains to be dated.

The Raglan-2 sample has a central age of  $281 \pm 37$  Ma based on 27 apatite grains (Fig. 11). Unfortunately only a single track length was measured preventing a quantitative assessment of the thermal history through inverse modelling. However, AFT data reveal that the central age is much younger than most of published AFT ages in the Canadian Shield (Pinet and Brake, 2018). On the radial plot (Fig. 11) grain data can be divided in two populations with a peak at 295 Ma and a less well defined peak at 112 Ma.

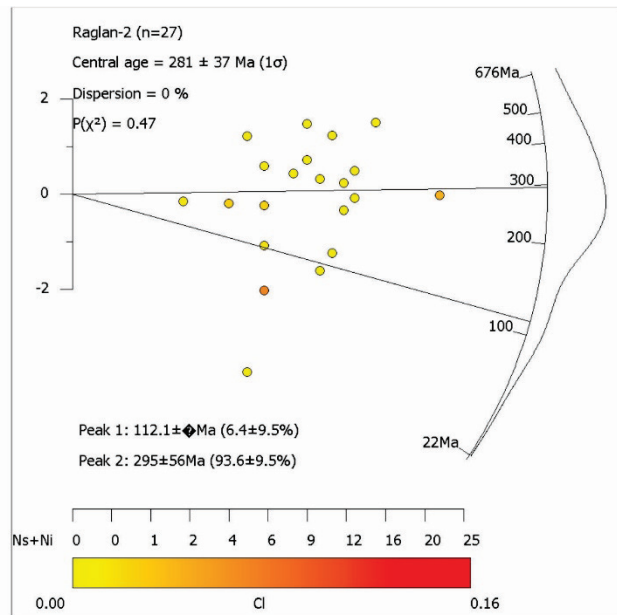


*Figure 11: Radial plot of the Raglan-2 sample. On this diagram, more precise fission-track ages plot further from the origin along the x-axis (precision). Radial plot done using the Radial Plotter software (Vermeesch, 2009).*

The presence of single grain ages < 200 Ma bear similarities with results from a sample collected on Akpatok Island at a depth of 340 m, 310 km to the east (central age  $230.6 \pm 13.5$  Ma; Pinet et al., 2016). However, when reported on a AFT age vs depth diagram (Fig. 12), the central age of the Raglan sample is comparable with those from Sudbury and LaRonde mine located at similar depths.

## **8. Discussion**

### *8a- Sampling strategy*

AFT data presented in this study aimed to document thermochronological history of samples located on three vertical profiles (Musselwhite, Raglan and Roberto mines). This aim was incompletely achieved for the Musselwhite and Roberto mines because crushed samples from surface (Musselwhite mine) or depth (down to -805 m in the Roberto mine) did not yield apatite, which restricted the extent of the analyzed vertical profiles. Adding new samples from these sites may provide weight to the presented interpretation and should be considered. In the Raglan mine, mafic and ultramafic rocks have poor apatite yields and prevent a detailed appraisal of a vertical profile. Meadowbank mine is an open pit and deep drill holes were not available for this study.

AFT results also show that iron formation (Musselwhite) and greywacke (Roberto) are appropriate lithologies for AFT dating. Apatites from these two sites are monocompositional and correspond to near end-member fluorapatite. A negative correlation of single grain apatite ages with Uranium content has been documented in Musselwhite and Meadowbank mines, but not in the Roberto Mine. This negative correlation and the overdispersion of single-grain AFT ages in monocompositional fluorapatites (i.e, low retentivity apatites) suggests that, in some cases, radiation damage affects the AFT chronometer, especially in slowly cooling terranes (McDannell et al., 2019a). However, the way radiation damage should be taken into account during inverse modelling remains controversial.

### *8b- Regional significance of AFT results*

Review of the quantitative burial/exhumation patterns at the scale of the Canadian Shield is beyond the scope of this study and only a brief comparison between AFT analyses from this study and published datasets will be presented.

Paleozoic subsidence over part of the Canadian Shield is attested by the sedimentary record of the Hudson Bay Basin and satellite basins. Several lines of evidence (including subsidence analysis, sedimentary xenoliths in kimberlites pipes and organic maturation data; see Pinet et al., 2013 for a review) indicate that the present-day basin outlines are erosional limits only and that sedimentary units have been deposited over vast areas and subsequently eroded away. However, the thickness, age and geographical distribution of such a paleo-sedimentary cover remain poorly constrained. Significant ( $> 20^{\circ}\text{C}$ ) temperature increases during the Phanerozoic that are most likely associated with sedimentary burial have also been documented through AFT studies in southern Ontario (Lorenzak et al., 2004), southeastern (Feinstein et al., 2009) and eastern (Pinet et al., 2016) Manitoba, northern Saskatchewan (Flowers, 2009), Northwest Territories (Ault et al., 2009 and 2013; Kohlmann, 2010), southern Baffin Island (McDannell et al., 2019b) and Hudson Strait (Pinet et al., 2016). This is in marked contrast with results for Musselwhite mine presented in this study. Our inverse modelling results using both HeFTy and QTQt modeling softwares indicate that such an episode of Phanerozoic heating was less pronounced ( $< 20^{\circ}\text{C}$ ) or negligible over the Musselwhite mine (and possibly the Meadowbank mine), even with models ‘forcing’ an increase in temperature during the 450-350 Ma period. This translates in significantly older ages compared to samples from Sudbury (Lorenzak et al., 2004) and LaRonde mine (Pinet, 2018) located at similar depths (Fig. 12). This clearly indicates that the Canadian Shield did not react as a single entity during the last billion years.

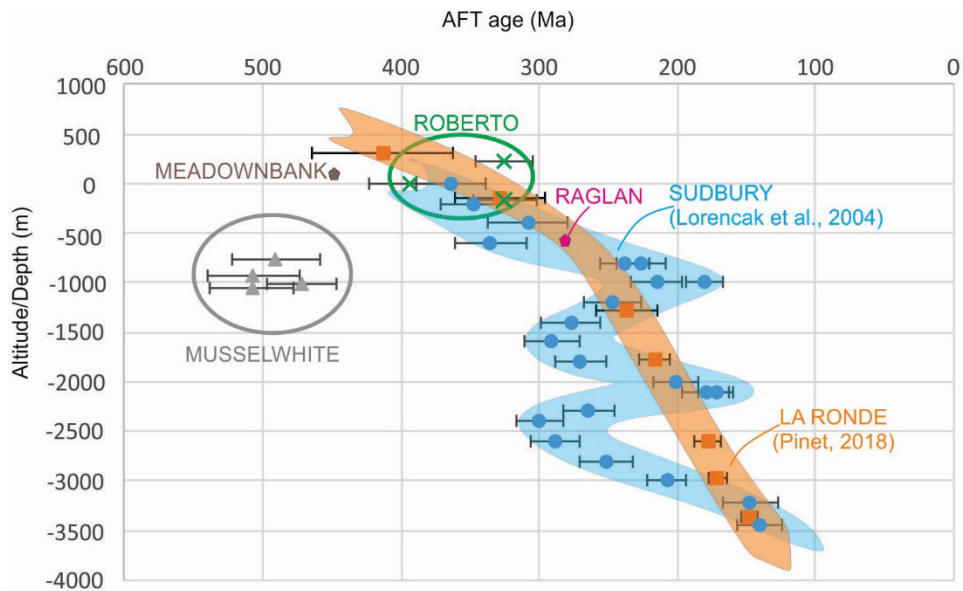


*Figure 12: AFT age versus altitude/depth for two plurikilometric vertical profiles (Sudbury, Lorenzak et al, 2004; LaRonde, Pinet, 2018). Note that the samples from the Musselwhite mine are significantly older than samples from Sudbury or LaRonde mine located at similar depths.*

Results from the Roberto mine illustrate the difficulty to model AFT data in the absence of geological evidence and independent geochronometers. In this case, the model in which samples were located relatively close to surface ( $35 < \text{temperature} < 70^\circ\text{C}$ ) at *ca* 500 Ma and then slightly heated during the Paleozoic better accounts for the partial annealing of some apatite grains, but remains to be better documented.

Interpretation of new (McDannell, *in press*) and published AFT data over the Canadian Shield should result in a better understanding of exhumation/subsidence patterns in time and space. These patterns will be compared with: 1) the boundaries of Precambrian Terranes (Percival et al., 2012) brought together during a series of Paleoproterozoic to Mesoproterozoic orogenic events; 2) the positive physiographic elements inferred to have influenced Paleozoic sedimentation (i.e., the arches of Sandford, 1987); 3) the present-day lithospheric architecture (crustal and/or lithospheric thickness, heat flow domains...) or 4) the position compared to Phanerozoic deforming zones. These comparisons may potentially challenge/add complexity to the ‘stability paradigm’ associated with cratons worldwide.

## **9. Acknowledgments**

Williams Oswald, Arnaud Fontaine, Vivien Janvier and Daniel Patry are thanked for providing the samples. Without their help, this study would not have been possible. Thanks also to Denis Lavoie for his support during the GEM program and Virginia Brake for the internal review of the manuscript.

## **10. References**

- Ault, A.K., Flowers, R.M., Bowring, S.A., 2009. Phanerozoic burial and unroofing history of the western Slave craton and Wopmay orogeny from apatite (U-Th)/He thermochronometry. *Earth and Planetary Science Letters*, 284, 1-11.
- Ault, A.K., Flowers, R.M., Bowring, S.A., 2013. Phanerozoic surface history of the Slave craton. *Tectonics*, 32, 1066-1083.
- Burtner, R. L., Nigrini, A., Donelick, R. A., 1994. Thermochronology of Lower Cretaceous source rocks in the Idaho-Wyoming thrust belt. *American Association Petroleum Geology Bulletin*, 78, 1613-1636.
- Carlson, W.D., Donelick, R.A., Ketcham, R.A., 1999. Variability of apatite fission-track annealing kinetics: I. Experimental results. *American Mineralogist*, 84, 1213-1223.
- Donelick, R.A., O'Sullivan, P.B., Ketcham, R.A., 2005. Apatite fission track analysis. *Reviews in Mineralogy and Geochemistry*, 58, 49-94.
- Feinstein, S., Kohn, B., Osadetz, K., Everitt, R., O'Sullivan, P., 2009. Variable Phanerozoic history in the southern Canadian Shield: evidence from an apatite fission track profile at the Underground Research Laboratory (URL), Manitoba. *Tectonophysics*, 475, 190-199.
- Flowers, R.M., 2009. Exploiting radiation damage control on apatite (U-Th)/He dates in cratonic regions. *Earth and Planetary Science Letters*, 277, 148-155.
- Fontaine, A., Dubé, B., Malo, M., McNicoll, V.J., Brisson, T., Doucet, D., and Goutier, J., 2015. Geology of the metamorphosed Roberto deposit (Éléonore mine), James Bay region, Quebec: diversity of mineralization styles in a polyphase tectonometamorphic setting, *In: Targeted Geoscience Initiative 4: Contributions to the understanding of Precambrian lode gold deposits and implication for exploration*, (ed) B. Dubé and P. Mercier-Langevin, Geological Survey of Canada Open File 7852, p. 209-225.
- Gallagher, K., 2012. Transdimensional inverse thermal history modeling for quantitative thermochronology. *Journal of Geophysical Research*, 117, B02408.

- Gallagher, K., Brown, R., Johnson, C., 1998. Fission track analysis and its applications to geological problems. *Annual Review Earth and Planetary Sciences*, 26, 519-572.
- Gallagher, K., Ketcham, R.A., 2018. Comment on 'Thermal history modelling: HeFTy vs QTQt' by Vermeesch and Tian. *Earth Science Reviews*, 176, 387-394.
- Gleadow, A.J.W., Belton, D.X., Kohn, B.P., Brown, R.W., 2002. Fission track dating of phosphate minerals and the thermochronology of apatite. In Kohn, M., Rakovan, J. and Hugues, J.M. (eds.) *Phosphates – Geochemical, Geobiological and Material importance, Reviews in Mineralogy and Geochemistry*, 48, 579-630.
- Green, P.F., Duddy, I.R., Gleadow, A.J.W., Tingate, P.R., Laslett, G.M., 1985. Fission track annealing in apatite track length measurements and the form of the Arrhenius plot. *Nuclear Tracks*, 10, 323-328.
- Green, P.F., Duddy, I.R., 2012. Thermal history reconstruction in sedimentary basins using apatite fission-track analysis and related techniques. In: *Analysing the thermal history of sedimentary basins: method and case studies*, SEPM Special Publication No 103, p. 65-104.
- Janvier, V., Castonguay, S., Mercier-Langevin, P., Dubé, B., Malo, M., McNicoll, V.J., Creaser, R.A., de Chavigny, B., and Pershson, S.J., 2015. Geology of the banded iron formation-hosted Meadowbank gold deposit, Churchill Province, Nunavut, In: *Targeted Geoscience Initiative 4: Contributions to the understanding of Precambrian lode gold deposits and implication for exploration*, (ed) B. Dubé and P. Mercier-Langevin, Geological Survey of Canada Open File 7852, p. 255-269.
- Ketcham, R.A., 2005. Forward and inverse modeling of low-temperature thermochronometry data. *Review in Mineralogy and Geochemistry*, 58, 275-314.
- Ketcham, R.A., 2013. HeFTy, version 1.8.2. Manual user dated 2 october 2013.
- Kohlmann, F., 2010. Insights into the nanoscale formation of fission tracks in solids and a low temperature thermochronology study of the Archean Slave province, Northwestern Territories, Canada. Ph. D Thesis, Univ. Melbourne (Australia), 302 p.
- Lavoie, D., Pinet, N., Dietrich, J., Chen, Z., 2015. The Paleozoic Hudson Bay Basin in northern Canada: new insights into hydrocarbon potential of a frontier intracratonic basin: *American Association of Petroleum Geologist Bulletin*, 99, 859-888.
- Lesher, C.M., 2007. Ni-Cu-(PGE) deposits in the Raglan area, Cape Smith Belt, New Quebec, In: Goodfellow, W.D., ed., *Mineral deposits of Canada: a synthesis of major deposit-types, district metallogeny, the evolution of geological provinces, and exploration methods: Special Publication No 5*, Mineral Deposits division, Geological Association of Canada, p. 351-386.

- Lorenzak, M., Kohn, B.P., Osadetz, K.G., Gleadow, A.J.W., 2004. Combined apatite fission-track and (U-Th)/He thermochronometry in a slowly cooled terrane: result from a 3340-m deep drill hole in the southern Canadian Shield. *Earth and Planetary Science Letters*, 227, 87-104.
- Malusà, M.G., Fitzgerald, P.G. (eds), 2019. *Fission-track thermochronology and its application to geology*. Springer textbooks in Earth Sciences and Environment, 393p.
- McDannell, K.T., Zeitler, P.K., Schneider, D.A., 2018. Instability of the southern Canadian Shield during the late Proterozoic. *Earth and Planetary Science Letters*, 490, 100-109.
- McDannell, K.T., Issler, D.R., O'Sullivan, P.B., 2019a. Radiation-enhanced fission track annealing revisited and consequences for apatite thermochronometry. *Geochimica et Cosmochimica Acta*, 252, 213-259.
- McDannell, K.T., Schneider, D.A., P.K., O'Sullivan, P.B., Issler, D.R., 2019b. Reconstructing deep-time histories from integrated thermochronology: an example from southern Baffin Island, Canada. *Terra Nova*, 31, 189-204.
- McDannell, K.T., Pinet, N., Issler, D.R., 2020, in press. Exhuming the Canadian Shield: Preliminary interpretations from low-temperature thermochronology and significance for the sedimentary succession of the Hudson Bay Basin, Chapter 8. *In: Sedimentary basins of the Canadian North - Contributions to a 1000 Ma geological journey and insight on resource potential*, Geological Survey of Canada Bulletin 609.
- Oswald, W., Castonguay, S., Dubé, B., McNicoll, V.J., Biczok, J., Malo, M., Mercier-Langevin, P., 2015. Geological setting of the world-class Musselwhite gold mine, Superior Province, northwestern Ontario: implication for exploration, *In: Targeted Geoscience Initiative 4: Contributions to the understanding of Precambrian lode gold deposits and implication for exploration*, (ed) B. Dubé and P. Mercier-Langevin, Geological Survey of Canada Open File 7852, p. 69-84.
- Percival, J.A., Skulski, T., Sanborn-Barrie, M., Stott, G.M., Leclair, A.D., Corkery, M.T., Boily, M., 2012. Geology and tectonic evolution of the Superior Province, Canada. Chapter 6 *In: Tectonic styles in Canada: the LITHOPROBE perspective*. Edited by J.A. Percival, F.A. Cook, and R.M. Clowes. Geological Association of Canada, Special Paper 49, pp. 321-378.
- Pinet, N., Lavoie, D., Dietrich, J., Hu, K., Keating, P., 2013. Architecture and subsidence history of the Hudson Bay intracratonic basin. *Earth-Science Review*, 125, 1-23.
- Pinet, N., Kohn, B.P., Lavoie, D., 2016. The ups and downs of the Canadian Shield: 1- preliminary results of apatite fission track analysis from the Hudson Bay region. Geological Survey of Canada, Open File 8110, 59 p.
- Pinet, N., 2018. The ups and downs of the Canadian Shield: 2- preliminary results of apatite fission-track analysis from a 3.6 km vertical profile, LaRonde mine, Quebec. Geological

Survey of Canada, open file 8385, 44 p.

Pinet, N., Brake, V., 2018. Preliminary compilation of apatite fission-track data in Canada. Open File 8454, 1 poster.

Sanford, B.V., 1987. Paleozoic geology of the Hudson platform. *In*: Beaumont, C. and Tankard, A.J. (eds), Sedimentary basins and basin-forming mechanisms, Canadian Society of Petroleum Geologists, Memoir 12, p. 483-505.

Vermeesch, P., 2009. RadialPlotter: a Java application for fission track, luminescence and other radial plots. *Radiation Measurements*, 44, 4, 409-410.

Vermeesch, P., Tian, Y., 2014. Thermal history modelling: HeFTy vs. QTQt. *Earth Science Reviews*, 139, 279-290.

## SAMPLE MW12-UG-105

Age: Archean  
type: Iron Formation

Easting : 90°21'49" (approximate)  
Northing: 52°36'46" (approximate)  
Elevation: -170 m

### GRAIN\_DATA

Number of grains                    20  
Number of Dpars                    80

Grain#	Ns	Ni	# square	MDpar	MDprp	U (ppm)	AFT age
1	29	10	15	3.2	1.419	8	630.8
2	54	23	15	3.454	1.479	18	515.3
3	14	8	8	3.052	1.301	12	388.0
4	36	13	12	3.105	1.231	13	603.6
5	56	23	28	2.94	1.338	10	533.6
6	41	18	15	3.063	1.766	14	500.5
7	29	14	12	3.063	1.419	13	456.8
8	39	14	10	2.918	1.535	16	607.0
9	13	8	10	2.511	1.262	9	361.0
10	87	29	24	2.88	1.317	14	651.4
11	45	20	27	2.652	1.144	9	494.7
12	31	22	18	2.599	1.499	14	314.2
13	86	40	20	2.826	1.411	23	473.5
14	87	43	32	3.104	1.232	16	446.5
15	83	38	40	2.461	1.316	11	480.7
16	15	8	9	2.96	1.595	10	414.8
17	67	40	35	2.852	1.211	13	371.8
18	45	11	28	3.039	1.573	5	872.9
19	37	17	15	2.621	1.324	13	479.1
20	16	9	12	2.73	1.543	9	393.9

### LENGTH\_DATA

Number\_of\_lens                    11  
Number\_of\_dpar                    28

#	Grain Nb	Len	Type	MDpar	MDprp	NDpar
1	2	12.8	T	3.069	1.451	4
2		8.677	T	2.988	1.54	4
3	8	8.361	T	2.964	1.311	4
4	8	12.124	T	2.964	1.311	0
5	8	10.498	T	2.964	1.311	0
6	8	13.038	T	2.964	1.311	0
7		11.212	T	3.14	1.749	4
8		9.773	T	2.539	1.148	4
9	18	13.825	T	2.815	1.332	4
10		12.583	T	2.815	1.332	0
11	20	9.392	T	2.736	1.418	4

## MICROPROBE DATA

---

### MASS PERCENT

Grain No.	P2O5	La2O3	F	SiO2	Cl	CaO	Na2O	SrO	FeO	MnO	Total
1	41.592	0.000	3.174	0	0.009	55.541	0.017	0	0.025	0.036	99.079
2	41.469	0.000	2.667	0	0.003	54.569	0.010	0	0.113	0.023	97.730
3	41.786	0.036	2.739	0	0.006	56.302	0.023	0	0.044	0.006	99.788
4	41.275	0.000	2.815	0	0.002	55.656	0.010	0	0.032	0.014	98.619
5	41.710	0.000	2.799	0	0.014	55.375	0.026	0	0.041	0.008	98.849
6	42.481	0.059	2.402	0	0.018	55.989	0.009	0	0.039	0.005	100.018
7	41.750	0.000	3.016	0	0.001	55.080	0.044	0	0.060	0.039	98.756
8	42.578	0.057	3.795	0	0.007	55.022	0.000	0	0.073	0.033	99.965
9	41.750	0.000	2.864	0	0.002	55.322	0.039	0	0.048	0.000	98.875
10	42.056	0.072	2.778	0	0.000	55.581	0.006	0	0.048	0.000	99.432
11	41.872	0.000	3.169	0	0.010	55.066	0.000	0	0.028	0.026	98.868
12	42.603	0.000	2.996	0	0.009	55.921	0.000	0	0.055	0.052	100.406
13	41.315	0.000	2.953	0	0.010	55.606	0.021	0	0.061	0.000	98.721
14	41.689	0.000	2.680	0	0.016	55.317	0.026	0	0.020	0.017	98.653
15	42.317	0.000	2.695	0	0.006	55.191	0.002	0	0.058	0.047	99.210
16	41.955	0.000	2.551	0	0.008	55.198	0.034	0	0.000	0.008	98.678
17	42.034	0.000	2.750	0	0.009	55.164	0.000	0	0.100	0.063	99.049
18	41.882	0.037	2.580	0	0.010	55.566	0.011	0	0.020	0.001	99.037
19	41.942	0.024	2.899	0	0.006	55.532	0.018	0	0.021	0.032	99.300
20	41.756	0.038	2.783	0	0.009	55.332	0.038	0	0.035	0.008	98.888

### CATION TOTAL

Grain No.	P	La	F	Si	Cl	Ca	Na	Sr	Fe	Mn	Total
1	0.2385	0	0.0637	0	0.0001	0.4031	0.0002	0	0.0001	0.0002	0.706
2	0.2399	0	0.0545	0	0	0.3995	0.0001	0	0.0006	0.0001	0.6948
3	0.2377	0.0001	0.055	0	0.0001	0.4053	0.0003	0	0.0002	0	0.6987
4	0.2377	0	0.0571	0	0	0.4055	0.0001	0	0.0002	0.0001	0.7007
5	0.2391	0	0.0565	0	0.0001	0.4017	0.0003	0	0.0002	0	0.698
6	0.2398	0.0001	0.0482	0	0.0002	0.3999	0.0001	0	0.0002	0	0.6887
7	0.2396	0	0.0607	0	0	0.4	0.0006	0	0.0003	0.0002	0.7015
8	0.2416	0.0001	0.0744	0	0.0001	0.3951	0	0	0.0004	0.0002	0.712
9	0.2392	0	0.0578	0	0	0.4012	0.0005	0	0.0003	0	0.6992
10	0.2395	0.0002	0.0558	0	0	0.4005	0.0001	0	0.0003	0	0.6966
11	0.24	0	0.0635	0	0.0001	0.3995	0	0	0.0002	0.0002	0.7036
12	0.2401	0	0.0593	0	0.0001	0.3989	0	0	0.0003	0.0003	0.6992
13	0.2378	0	0.0597	0	0.0001	0.405	0.0003	0	0.0003	0	0.7032
14	0.2392	0	0.0543	0	0.0002	0.4016	0.0003	0	0.0001	0.0001	0.696
15	0.2408	0	0.0542	0	0.0001	0.3974	0	0	0.0003	0.0003	0.6933
16	0.24	0	0.0517	0	0.0001	0.3997	0.0004	0	0	0	0.6919
17	0.24	0	0.0554	0	0.0001	0.3987	0	0	0.0006	0.0004	0.6954
18	0.2392	0.0001	0.0522	0	0.0001	0.4016	0.0001	0	0.0001	0	0.6935
19	0.2393	0.0001	0.0582	0	0.0001	0.401	0.0002	0	0.0001	0.0002	0.6993
20	0.2392	0.0001	0.0562	0	0.0001	0.4011	0.0005	0	0.0002	0	0.6976

## SAMPLE MW12-UG-023

Age: Archean  
type: Iron Formation

Easting : 90°21'49" (approximate)  
Northing: 52°36'46" (approximate)  
Elevation: -920 m

### GRAIN DATA

	Number of grains 22							
	Number of Dpars 88							
Grain#	Ns	Ni	#square	MDpar	MDprp	U (ppm)	AFT age	
1	208	95	100	2.668	1.105	11	470.8	
2	12	5	15	2.221	1.107	4	514.3	
3	26	9	7	2.765	1.158	15	614.2	
4	30	13	30	2.231	1.051	5	495.2	
5	10	6	16	2.656	1.117	4	361.4	
6	20	6	12	2.37	0.981	6	703.7	
7	35	16	25	2.645	1.471	8	470.4	
8	16	6	15	3.092	1.621	5	569.0	
9	32	17	25	2.348	1.594	8	406.8	
10	39	16	16	2.375	1.136	12	522.0	
11	14	7	10	2.885	1.626	8	431.4	
12	11	6	12	2.811	2.023	6	396.5	
13	11	6	8	2.662	1.58	9	396.5	
14	26	15	21	2.429	1.254	8	375.5	
15	14	5	9	2.303	1.357	7	596.1	
16	59	17	60	2.299	1.282	3	731.1	
17	103	39	60	2.483	1.141	8	563.7	
18	39	16	18	2.468	1.03	11	522.0	
19	31	12	36	2.419	1.092	4	551.9	
20	68	30	32	2.635	1.002	11	486.8	
21	75	28	42	2.532	1.105	8	571.4	
22	36	16	48	2.514	1.103	4	483.3	

### LENGTH DATA

	Number_of_lens 11							
	Number_of_dpar 24							
#	Grain Nb	Len	Type	MDpar	MDprp	NDpar	Angle with C-	
1	1	14.275	T	2.72	1.208	4	62.438	
2	1	13.605	T	2.72	1.208	0	80.640	
3	1	9.345	T	2.72	1.208	0	69.784	
4	2	11.785	T	2.277	1.098	4	80.408	
5	3	9.761	T	2.364	1.183	4	72.792	
6	16	9.986	T	2.303	1.14	4	61.988	
7	19	14.023	T	2.416	1.138	4	63.860	
8	21	14.006	T	2.219	1.194	4	68.567	
9	21	10.581	T	2.219	1.194	0	32.190	
10	21	11.754	T	2.219	1.194	0	79.808	
11	21	11.173	T	2.219	1.194	0	53.217	

## MICROPROBE DATA

---

### MASS PERCENT

Grain No.	P2O5	La2O3	F	SiO2	Cl	CaO	Ce2O3	Na2O	SrO	FeO	MnO	Total
1	41.928	0.048	3.037	0	0.012	55.951	0.0740	0.009	0.000	0.026	0.040	99.843
2	42.326	0.000	2.624	0	0.011	55.575	0.0510	0.000	0.000	0.076	0.044	99.600
3	41.999	0.000	3.198	0	0.005	55.812	0.0430	0.005	0.000	0.084	0.021	99.819
4	41.969	0.000	2.589	0	0.006	55.499	0.0310	0.017	0.000	0.024	0.000	99.044
5	41.236	0.118	2.959	0	0.000	55.690	0.0200	0.010	0.000	0.068	0.000	98.855
6	41.646	0.009	3.057	0	0.034	55.195	0.0790	0.004	0.085	0.075	0.040	98.929
7	41.783	0.000	2.621	0	0.008	55.976	0.0560	0.024	0.000	0.033	0.000	99.395
8	41.293	0.000	2.637	0	0.039	55.402	0.0150	0.014	0.000	0.054	0.049	98.384
9	41.703	0.000	2.471	0	0.010	56.116	0.0560	0.000	0.000	0.002	0.014	99.330
10	41.539	0.024	2.956	0	0.001	55.968	0.0180	0.017	0.000	0.024	0.000	99.302
11	41.267	0.000	2.795	0	0.012	55.184	0.0050	0.007	0.000	0.065	0.024	98.179
12	40.810	0.000	2.753	0	0.015	55.943	0.0660	0.025	0.062	0.088	0.009	98.609
13	41.977	0.067	3.023	0	0.006	55.962	0.0030	0.015	0.000	0.000	0.041	99.820
14	41.494	0.000	2.832	0	0.004	54.831	0.0000	0.000	0.000	0.062	0.000	98.030
15	41.003	0.000	2.706	0	0.009	54.116	0.0030	0.000	0.000	0.065	0.027	96.788
16	42.017	0.000	2.819	0	0.004	54.086	0.0000	0.000	0.142	0.077	0.012	97.969
17	42.258	0.000	2.890	0	0.010	54.584	0.0000	0.008	0.000	0.039	0.006	98.576
18	42.297	0.000	2.910	0	0.014	54.878	0.1140	0.001	0.000	0.007	0.028	99.021
19	41.833	0.000	2.824	0	0.012	54.394	0.0840	0.016	0.000	0.031	0.024	98.026
20	42.520	0.097	3.198	0	0.011	55.213	0.0000	0.000	0.000	0.053	0.014	99.757
21	41.664	0.000	2.940	0	0.051	54.403	0.0660	0.010	0.000	0.064	0.016	97.964
22	42.045	0.000	2.996	0	0.010	54.079	0.0000	0.006	0.020	0.006	0.004	97.903

### CATION TOTAL

Grain No.	P	La	F	Si	Cl	Ca	Ce	Na	Sr	Fe	Mn	Total
1	0.2385	0.0001	0.0606	0	0.0001	0.4028	0.00020	0.0001	0.0000	0.0001	0.0002	0.7027
2	0.2401	0.0000	0.0527	0	0.0001	0.3989	0.00010	0.0000	0.0000	0.0004	0.0003	0.6927
3	0.2389	0.0000	0.0636	0	0.0001	0.4018	0.00010	0.0001	0.0000	0.0005	0.0001	0.7053
4	0.2395	0.0000	0.0523	0	0.0001	0.4008	0.00010	0.0002	0.0000	0.0001	0.0000	0.6931
5	0.2373	0.0003	0.0598	0	0.0000	0.4057	0.00010	0.0001	0.0000	0.0004	0.0000	0.7038
6	0.2391	0.0000	0.0615	0	0.0004	0.401	0.00020	0.0000	0.0003	0.0004	0.0002	0.7031
7	0.2382	0.0000	0.0529	0	0.0001	0.4039	0.00010	0.0003	0.0000	0.0002	0.0000	0.6957
8	0.238	0.0000	0.0537	0	0.0004	0.4042	0.00000	0.0002	0.0000	0.0003	0.0003	0.6971
9	0.2379	0.0000	0.05	0	0.0001	0.4051	0.00010	0.0000	0.0000	0.0000	0.0001	0.6934
10	0.2377	0.0001	0.0594	0	0.0000	0.4053	0.00000	0.0002	0.0000	0.0001	0.0000	0.7028
11	0.2384	0.0000	0.0569	0	0.0001	0.4034	0.00000	0.0001	0.0000	0.0004	0.0001	0.6995
12	0.2359	0.0000	0.0561	0	0.0002	0.4092	0.00020	0.0003	0.0002	0.0005	0.0001	0.7028
13	0.2387	0.0002	0.0603	0	0.0001	0.4027	0.00000	0.0002	0.0000	0.0000	0.0002	0.7024
14	0.2396	0.0000	0.0576	0	0.0000	0.4007	0.00000	0.0000	0.0000	0.0004	0.0000	0.6984
15	0.2397	0.0000	0.0558	0	0.0001	0.4003	0.00000	0.0000	0.0000	0.0004	0.0002	0.6965
16	0.2419	0.0000	0.0572	0	0.0000	0.3941	0.00000	0.0000	0.0006	0.0004	0.0001	0.6944
17	0.2418	0.0000	0.0582	0	0.0001	0.3952	0.00000	0.0001	0.0000	0.0002	0.0000	0.6956
18	0.2413	0.0000	0.0584	0	0.0002	0.3962	0.00030	0.0000	0.0000	0.0000	0.0002	0.6966
19	0.241	0.0000	0.0573	0	0.0001	0.3966	0.00020	0.0002	0.0000	0.0002	0.0001	0.6957
20	0.2412	0.0002	0.0635	0	0.0001	0.3963	0.00000	0.0000	0.0000	0.0003	0.0001	0.7017
21	0.2406	0.0000	0.0596	0	0.0006	0.3976	0.00020	0.0001	0.0000	0.0004	0.0001	0.6993
22	0.2422	0.0000	0.0606	0	0.0001	0.3943	0.00000	0.0001	0.0001	0.0000	0.0000	0.6975

## SAMPLE MW13-UG-010

Age: Archean  
rock type: Iron Formation

Easting : 90°21'49" (approximate)  
Northing: 52°36'46" (approximate)  
Elevation: -1020 m

### GRAIN\_DATA

---

Number of grains                    21  
Number of Dpars                    84

Grain#	Ns	Ni	# square	MDpar	MDprp	U (ppm)	AFT age
1	58	39	16	2.524	1.074	28	334
2	33	12	12	2.79	1.145	11	604
3	112	55	32	2.756	1.385	20	453
4	101	47	49	2.729	1.232	11	477
5	148	57	35	2.394	1.259	19	572
6	127	50	56	2.682	1.313	10	560
7	67	28	20	2.735	1.193	16	529
8	109	43	49	2.711	1.106	10	559
9	25	11	42	3.13	1.252	3	503
10	140	75	40	2.786	1.421	22	416
11	22	8	15	2.495	1.252	6	604
12	78	36	27	2.466	1.216	15	481
13	107	35	50	2.68	1.139	8	668
14	53	24	20	2.604	1.341	14	490
15	58	25	20	2.619	1.241	14	513
16	65	42	56	2.532	1.197	9	347
17	83	48	35	2.811	1.285	16	386
18	34	24	12	2.837	1.172	23	318
19	26	10	100	2.667	1.31	1	573
20	82	37	60	2.675	1.109	7	491
21	101	61	60	2.538	1.162	12	371

## **LENGTH\_DATA**

Number_of_lens	85						
Number_of_dpar	136						
#	Grain Nb	Len	Type	MDpar	MDprp	NDpar	Angle with C-
1	1	4.13	T	2.559	1.18	4	83.511
2	3	10.958	T	2.714	1.259	4	55.65
3	3	15.014	T	2.714	1.259	0	38.462
4	3	12.835	T	2.714	1.259	0	73.746
5		13.131	T	2.819	1.285	4	76.231
6		11.476	T	2.819	1.285	0	58.717
7		13.58	T	2.819	1.285	0	70.893
8		12.309	T	2.819	1.285	0	67.223
9		8.211	T	2.618	1.259	4	50.337
10	1	13.842	T	2.725	1.198	4	75.77
11	1	11.161	T	2.791	1.207	4	74.681
12	10	12.622	T	2.834	1.192	4	87.178
13	10	14.067	T	2.89	1.33	4	46.27
14	10	12.288	T	2.89	1.33	0	54.413
15	10	10.145	T	2.89	1.33	0	88.568
16	10	13.144	T	2.89	1.33	0	85.299
17	10	11.456	T	2.89	1.33	0	68.459
18	10	12.667	T	2.89	1.33	0	83.718
19		13.996	T	2.693	1.197	4	65.046
20		9.717	T	2.693	1.197	0	81.743
21		12.783	T	2.693	1.197	0	47.39
22		10.512	T	2.693	1.197	0	83.51
23	13	14.617	T	2.58	1.265	4	82.642
24	13	12.018	T	2.58	1.265	0	77.557
25		12.12	T	2.616	1.204	4	87.677
26		9.972	T	2.616	1.204	0	46.443
27		11.658	T	2.616	1.204	0	53.982
28		11.81	T	2.607	1.109	4	64.18
29		14.656	T	2.806	1.414	4	74.73
30	17	13.368	T	2.811	1.181	4	73.721
31	17	11.738	T	2.811	1.181	0	88.046
32	17	11.346	T	2.811	1.181	0	56.994
33	17	13.211	T	2.811	1.181	0	46.259
34		10.234	T	2.707	1.3	4	52.865
35		14.123	T	2.538	1.144	4	68.04
36		12.543	T	2.527	1.238	4	60.812

37	14.302	T	2.496	1.294	4	49.334
38	3.707	T	2.575	1.099	4	80.557
39	12.7	T	2.662	1	4	60.923
40	11.662	T	2.662	1	0	84.173
41	13.051	T	2.662	1	0	70.716
42	9.317	T	2.353	1.097	4	81.758
43	10.863	T	2.585	1.175	4	48.513
44	7.04	T	2.585	1.175	0	73.808
45	13.271	T	2.585	1.175	0	65.189
46	10.033	T	2.628	1.152	4	89.895
47	13.475	T	2.628	1.152	0	77.576
48	14.155	T	2.628	1.152	0	69.128
49	10.196	T	2.628	1.152	0	84.706
50	10.656	T	2.628	1.152	0	60.657
51	9.44	T	2.628	1.152	0	56.634
52	11.914	T	2.628	1.152	0	59.617
53	10.96	T	2.665	1.21	4	53.566
54	12.707	T	2.665	1.21	0	72.836
55	12.424	T	2.665	1.21	0	50.392
56	10.342	T	2.736	1.161	4	69.912
57	9.164	T	2.596	1.339	4	50.716
58	13.321	T	2.596	1.339	0	58.968
59	14.227	T	2.596	1.339	0	64.454
60	11.31	T	2.596	1.339	0	81.823
61	14.126	T	2.596	1.339	0	72.64
62	16.28	T	2.764	1.118	4	85.588
63	13.646	T	2.69	1.181	4	73.766
64	14.378	T	2.69	1.181	0	68.998
65	11.961	T	2.69	1.181	0	65.899
66	8.362	T	2.534	1.253	4	73.931
67	8.447	T	2.534	1.253	0	84.398
68	12.544	T	2.534	1.253	0	50.086
69	12.39	T	2.414	1.236	4	50.881
70	9.291	T	2.414	1.236	0	79.548
71	11.943	T	2.414	1.236	0	57.939
72	10.526	T	2.414	1.236	0	39.161
73	12.028	T	2.468	1.105	4	81.167
74	10.163	T	2.468	1.105	0	50.102
75	11.446	T	2.468	1.105	0	61.961
76	10.097	T	2.468	1.105	0	50.102
77	13.464	T	2.637	1.059	4	73.877
78	13.397	T	2.637	1.059	0	74.681
79	10.383	T	2.73	1.249	4	81.402
80	12.482	T	2.73	1.249	0	70.049
81	11.607	T	2.73	1.249	0	74.633
82	15.193	T	2.73	1.249	0	54.204
83	11.919	T	2.53	1.084	4	82.853
84	9.134	T	2.53	1.084	0	63.336
85	11.539	T	2.53	1.084	0	78.736

## MICROPROBE DATA

---

### (1) MASS PERCENT

Grain No.	P2O5	La2O3	F	SiO2	Cl	CaO	Ce2O3	Na2O	SrO	FeO	MnO	Total
1	41.832	0.091	2.564	0	0.010	55.003	0.050	0.011	0	0.028	0.040	98.547
2	41.074	0.000	2.521	0	0.009	54.434	0.021	0.043	0	0.045	0.031	97.115
3	40.687	0.000	2.801	0	0.017	53.051	0.000	0.093	0	0.032	0.000	95.498
4	41.239	0.066	2.768	0	0.010	54.741	0.005	0.035	0	0.048	0.000	97.745
5	41.053	0.000	2.510	0	0.010	55.156	0.000	0.003	0	0.030	0.000	97.703
6	40.499	0.000	2.763	0	0.015	54.811	0.000	0.028	0	0.019	0.024	96.993
7	41.488	0.000	2.697	0	0.010	54.844	0.021	0.027	0.064	0.077	0.049	98.139
8	41.131	0.031	3.068	0	0.006	54.480	0.003	0.000	0	0.081	0.000	97.507
9	40.989	0.000	2.417	0	0.018	54.487	0.000	0.000	0	0.052	0.007	96.948
10	40.894	0.000	3.004	0	0.009	54.714	0.010	0.005	0	0.049	0.055	97.473
11	41.199	0.079	3.002	0	0.010	55.637	0.063	0.000	0	0.008	0.000	98.732
12	41.249	0.074	2.933	0	0.005	55.368	0.081	0.010	0	0.014	0.014	98.512
13	41.144	0.000	2.920	0	0.011	54.566	0.000	0.003	0	0.063	0.000	97.476
14	41.383	0.011	3.000	0	0.006	55.159	0.000	0.006	0	0.016	0.000	98.317
15	41.389	0.000	3.016	0	0.017	55.277	0.000	0.017	0	0.021	0.000	98.463
16	41.083	0.068	2.706	0	0.013	55.162	0.057	0.000	0	0.000	0.006	97.953
17	41.130	0.000	2.909	0	0.010	54.691	0.044	0.000	0	0.000	0.000	97.557
18	41.477	0.005	2.675	0	0.013	55.621	0.000	0.006	0	0.066	0.000	98.734
19	41.085	0.025	2.287	0	0.043	55.112	0.018	0.000	0	0.000	0.016	97.613
20	41.241	0.073	2.641	0	0.011	55.639	0.023	0.011	0	0.026	0.000	98.551
21	41.007	0.038	2.646	0	0.017	55.394	0.000	0.000	0	0.008	0.000	97.992

### (2) CATION TOTAL

Grain No.	P	La	F	Si	Cl	Ca	Ce	Na	Sr	Fe	Mn	Total
1	0.2399	0.0002	0.0521	0	0.0001	0.3992	0.0001	0.0001	0	0.0002	0.0002	0.6921
2	0.2392	0	0.052	0	0.0001	0.4012	0.0001	0.0006	0	0.0003	0.0002	0.6937
3	0.2408	0	0.0583	0	0.0002	0.3973	0	0.0013	0	0.0002	0	0.6981
4	0.2391	0.0002	0.0565	0	0.0001	0.4016	0	0.0005	0	0.0003	0	0.6984
5	0.238	0	0.0515	0	0.0001	0.4047	0	0	0	0.0002	0	0.6945
6	0.2373	0	0.057	0	0.0002	0.4064	0	0.0004	0	0.0001	0.0001	0.7016
7	0.2393	0	0.0549	0	0.0001	0.4004	0.0001	0.0004	0.0003	0.0004	0.0003	0.6963
8	0.2393	0.0001	0.0625	0	0.0001	0.4011	0	0	0	0.0005	0	0.7036
9	0.239	0	0.05	0	0.0002	0.4021	0	0	0	0.0003	0	0.6917
10	0.2383	0	0.0614	0	0.0001	0.4035	0	0.0001	0	0.0003	0.0003	0.7041
11	0.2374	0.0002	0.0607	0	0.0001	0.4058	0.0002	0	0	0	0	0.7045
12	0.238	0.0002	0.0595	0	0.0001	0.4042	0.0002	0.0001	0	0.0001	0.0001	0.7026
13	0.2392	0	0.0596	0	0.0001	0.4015	0	0	0	0.0004	0	0.7009
14	0.2388	0	0.0607	0	0.0001	0.4028	0	0.0001	0	0.0001	0	0.7027
15	0.2386	0	0.061	0	0.0002	0.4033	0	0.0002	0	0.0001	0	0.7034
16	0.238	0.0002	0.0553	0	0.0001	0.4044	0.0001	0	0	0	0	0.6981
17	0.239	0	0.0594	0	0.0001	0.4022	0.0001	0	0	0	0	0.7009
18	0.2382	0	0.0542	0	0.0001	0.4042	0	0.0001	0	0.0004	0	0.6973
19	0.2382	0.0001	0.0472	0	0.0005	0.4043	0	0	0	0	0.0001	0.6905
20	0.2375	0.0002	0.0538	0	0.0001	0.4056	0.0001	0.0001	0	0.0001	0	0.6976
21	0.2375	0.0001	0.0541	0	0.0002	0.406	0	0	0	0	0	0.698

## SAMPLE MW13-UG-018

Age: Archean  
 rock type: Iron Formation

Easting : 90°21'49" (approximate)  
 Northing: 52°36'46" (approximate)  
 Elevation: -1045 m

### GRAIN\_DATA

Number of grains	19							
Number of Dpars	76							
Grain#	Ns	Ni	# square	MDpar	MDprp	U (ppm)	AFT age	
1	49	21	49	2.528	1.322	5	531.8	
2	194	85	100	2.185	1.066	10	520.6	
3	34	18	40	2.454	1.194	5	433.8	
4	223	63	42	2.527	1.148	17	790.4	
5	10	6	15	2.498	1.168	5	384.3	
6	40	17	27	2.415	1.14	7	536.1	
7	96	35	24	2.256	1.11	17	620.7	
8	25	8	28	2.439	0.983	3	702.7	
9	27	10	16	2.501	0.873	7	611.5	
10	138	59	100	2.417	0.977	7	533.0	
11	55	22	20	2.522	1.144	13	568.1	
12	106	49	40	2.384	1.136	14	494.5	
13	86	46	35	2.596	1.197	15	429.5	
14	39	16	49	2.506	0.988	4	554.5	
15	53	29	45	2.391	1.216	7	420.2	
16	194	89	100	2.612	1.121	10	498.1	
17	19	8	15	2.724	1.114	6	540.9	
18	38	20	70	2.594	1.201	3	436.3	
19	456	239	100	2.371	1.045	27	438.0	

### LENGTH\_DATA

Number_of_lens	18
Number_of_dpar	24

#	Grain Nb	Len	Type	MDpar	MDprp	NDpar	Angle witl
1	3	11.065	T	2.418	1.167	4	74.42
2	3	11.057	T	2.66	0.982	4	58.94
3	13	10.476	T	2.716	1.183	4	59.711
4	13	11.351	T	2.716	1.183	0	61.31
5	13	8.3	T	2.716	1.183	0	75.759
6	13	7.911	T	2.716	1.183	0	85.354
7	16	11.098	T	2.526	1.162	4	39.719
8	16	15.504	T	2.526	1.162	0	45.711
9	2	14.557	T	2.557	1.089	4	38.838
10	2	9.515	T	2.557	1.089	0	77.078
11	2	7.248	T	2.557	1.089	0	59.499
12	2	12.562	T	2.557	1.089	0	54.557
13	2	11.737	T	2.557	1.089	0	79.786
14	2	12.917	T	2.563	1.086	0	51.516
15	2	14.213	T	2.563	1.086	0	59.877
16	2	14.609	T	2.563	1.086	0	45.295
17	2	14.462	T	2.563	1.086	0	66.866
18	2	14.358	T	2.563	1.086	4	32.061

## MICROPROBE DATA

---

### (1) MASS PERCENT

Grain No.	P2O5	La2O3	F	SiO2	Cl	CaO	Ce2O3	Na2O	SrO	FeO	MnO	Total
1	41.246	0.015	2.706	0	0.02	55.25	0.050	0.01	0	0.009	0.025	98.188
2	41.495	0.000	2.972	0	0.01	53.79	0.099	0.05	0	0.017	0.028	97.206
3	41.738	0.000	2.702	0	0.01	54.32	0.000	0.03	0	0.047	0.033	97.739
4	40.798	0.000	2.928	0	0.02	54.90	0.000	0.10	0	0.087	0.000	97.591
5	41.434	0.000	2.753	0	0.01	55.76	0.031	0.03	0	0.049	0.020	98.925
6	41.951	0.091	2.593	0	0.02	55.20	0.039	0.01	0	0.031	0.024	98.866
7	41.577	0.000	2.630	0	0.01	55.81	0.107	0.09	0	0.038	0.033	99.182
8	40.962	0.087	2.730	0	0.02	55.40	0.024	0.02	0	0.010	0.000	98.099
9	41.737	0.047	2.554	0	0.02	54.64	0.013	0.02	0	0.069	0.051	98.065
10	41.246	0.089	2.783	0	0.01	55.55	0.039	0.03	0	0.001	0.060	98.633
11	41.324	0.050	2.788	0	0.01	56.72	0.000	0.00	0	0.064	0.015	99.798
12	41.213	0.000	2.822	0	0.02	55.04	0.065	0.03	0	0.078	0.005	98.075
13	41.477	0.052	2.551	0	0.01	55.12	0.126	0.08	0	0.029	0.042	98.410
14	41.529	0.000	2.885	0	0.01	55.82	0.000	0.02	0	0.043	0.027	99.116
15	41.105	0.000	2.622	0	0.02	54.79	0.000	0.06	0	0.069	0.001	97.551
16	41.482	0.000	2.770	0	0.01	54.25	0.021	0.05	0	0.062	0.045	97.520
17	41.404	0.000	3.218	0	0.02	55.48	0.029	0.00	0	0.030	0.002	98.826
18	41.521	0.000	2.697	0	0.02	55.26	0.000	0.00	0	0.028	0.009	98.389
19	41.673	0.077	3.044	0	0.01	55.26	0.000	0.00	0	0.035	0.043	98.858

### | CATION TOTAL

No.	P	La	F	Si	Cl	Ca	Ce	Na	Sr	Fe	Mn	Total
1	0.2382	0	0.0552	0	0.0002	0.4039	0.0001	0.0001	0	0.0001	0.0001	0.698
2	0.2413	0	0.0606	0	0.0001	0.3958	0.0003	0.0006	0	0.0001	0.0002	0.699
3	0.241	0	0.0551	0	0.0001	0.3969	0	0.0004	0	0.0003	0.0002	0.694
4	0.2377	0	0.0599	0	0.0002	0.4047	0	0.0014	0	0.0005	0	0.7045
5	0.2378	0	0.0557	0	0.0001	0.4049	0.0001	0.0003	0	0.0003	0.0001	0.6994
6	0.2399	0.0002	0.0525	0	0.0002	0.3994	0.0001	0.0001	0	0.0002	0.0001	0.6928
7	0.2378	0	0.0532	0	0.0001	0.404	0.0003	0.0012	0	0.0002	0.0002	0.697
8	0.2373	0.0002	0.0558	0	0.0002	0.4061	0.0001	0.0003	0	0.0001	0	0.7002
9	0.2403	0.0001	0.0521	0	0.0002	0.3981	0	0.0002	0	0.0004	0.0003	0.6917
10	0.2376	0.0002	0.0565	0	0.0001	0.405	0.0001	0.0004	0	0	0.0003	0.7002
11	0.2359	0.0001	0.0561	0	0.0001	0.4097	0	0	0	0.0004	0.0001	0.7025
12	0.2384	0	0.0575	0	0.0002	0.403	0.0002	0.0004	0	0.0004	0	0.7002
13	0.2388	0.0001	0.052	0	0.0002	0.4015	0.0003	0.0011	0	0.0002	0.0002	0.6944
14	0.2379	0	0.0581	0	0.0001	0.4047	0	0.0003	0	0.0002	0.0002	0.7015
15	0.2387	0	0.0538	0	0.0002	0.4026	0	0.0007	0	0.0004	0	0.6964
16	0.2404	0	0.0566	0	0.0001	0.3979	0.0001	0.0007	0	0.0004	0.0003	0.6965
17	0.2383	0	0.0647	0	0.0002	0.4041	0.0001	0	0	0.0002	0	0.7077
18	0.2389	0	0.0548	0	0.0002	0.4024	0	0	0	0.0002	0.0001	0.6967
19	0.2392	0.0002	0.0612	0	0.0001	0.4014	0	0	0	0.0002	0.0002	0.7025

## SAMPLE RAGLAN2

Age: Archean  
Rock type gabbro

Coordinates

Easting -73.677  
Northing 61.6876  
Elevation -630

### **GRAIN\_DATA**

---

Number of grains	27
Number of Dpars	100

Grain#	Ns	Ni	#square	MDpar	MDprp	U (ppm)
1	2	4	10	2.281	0.926	4
2	1	1	8	2.424	1.077	1
3	6	3	28	2.41	0.844	1
4	6	4	18	2.246	1.05	2
5	8	5	24	2.272	0.897	2
6	11	4	20	2.362	0.959	2
7	6	6	18	2.282	0.989	4
8	7	2	16	2.247	1.046	1
9	5	3	15	2.517	1.004	2
10	2	4	24	2.279	0.943	2
11	4	2	9	2.356	0.907	2
12	5	3	24	2.177	1.036	1
13	3	7	24	2.653	1.017	3
14	1	1	15	2.278	0.941	1
15	2	2	6	2.245	0.925	4
16	4	7	25	2.169	1.006	3
17	12	10	40	2.574	0.971	3
18	4	1	24	2.591	0.838	0
19	3	3	12	2.621	0.91	3
20	7	5	12	2.312	1.085	5
21	2	2	8	2.215	0.947	3
22	1	5	24	2.296	0.975	2
23	0	5	12	2.006	1.125	5
24	4	1	18	2.282	0.855	1
25	8	3	30	2.328	1.035	1
26	7	6	28	2.155	0.953	2
27	6	6	30	2.267	1.032	2

### **LENGTH\_DATA**

---

Number_of_lens	1
Number_of_dpar	4

#	Len	Type	MDpar	MDprp	NDpar	Angle with C-axis
1	14.095	T	2.294	0.975	4	58.569

## MICROPROBE DATA

---

### MASS PERCENT

Grain No.	P2O5	La2O3	F	SiO2	Cl	CaO	Ce2O3	Na2O	SrO	FeO	MnO	Total
1	41.484	0.033	3.355	0.001	0.005	56.076	0.097	0.025	0	0.049	0.016	99.727
2	41.574	0.045	3.094	0.041	0.156	56.297	0.131	0.006	0	0.474	0.087	100.567
3	41.071	0.000	3.919	0.000	0.004	54.880	0.073	0.004	0	0.221	0.075	98.596
4	41.586	0.073	3.512	0.000	0.010	54.533	0.128	0.009	0	0.161	0.121	98.652
6	41.155	0.059	3.735	0.032	0.008	54.979	0.186	0.018	0	0.195	0.081	98.873
7	40.822	0.106	3.575	0.000	0.011	55.198	0.086	0.018	0	0.218	0.049	98.576
8	40.843	0.000	3.678	0.062	0.017	55.109	0.199	0.000	0	0.247	0.033	98.635
9	41.419	0.027	3.965	0.000	0.003	55.425	0.060	0.026	0	0.070	0.020	99.345
10	40.767	0.086	3.341	0.021	0.053	54.757	0.139	0.011	0	0.205	0.068	98.029
11	41.756	0.000	3.725	0.062	0.018	55.160	0.194	0.001	0	0.299	0.062	99.705
12	42.395	0.047	3.709	0.035	0.014	54.816	0.076	0.009	0	0.095	0.046	99.677
13	41.534	0.086	3.676	0.047	0.011	54.347	0.031	0.012	0	0.193	0.088	98.475
14	41.838	0.000	3.958	0.022	0.003	54.665	0.097	0.004	0	0.038	0.007	98.964
15	41.232	0.100	3.497	0.040	0.014	55.289	0.129	0.038	0	0.159	0.046	99.069
16	41.557	0.002	4.684	0.012	0.014	55.148	0.089	0.001	0	0.143	0.028	99.703
17	41.726	0.065	3.516	0.018	0.009	54.601	0.115	0.000	0	0.249	0.083	98.900
18	41.536	0.000	3.669	0.032	0.047	54.153	0.184	0.033	0	0.399	0.119	98.616
19	42.425	0.120	3.244	0.000	0.008	55.849	0.074	0.034	0	0.075	0.042	100.503
20	41.699	0.110	3.717	0.044	0.028	54.661	0.094	0.009	0	0.213	0.064	99.068
21	41.963	0.084	3.204	0.000	0.012	54.109	0.123	0.002	0	0.208	0.063	98.416
22	41.201	0.000	3.581	0.054	0.030	53.780	0.142	0.017	0	0.331	0.052	97.673
23	41.708	0.107	2.752	0.033	0.073	55.096	0.129	0.008	0	0.364	0.044	99.139
24	41.684	0.000	3.088	0.037	0.006	55.564	0.123	0.016	0	0.123	0.023	99.363
25	41.981	0.000	3.966	0.000	0.004	55.512	0.108	0.010	0	0.093	0.041	100.044
26	41.637	0.032	3.227	0.026	0.009	54.068	0.087	0.006	0	0.275	0.033	98.039
27	42.030	0.087	4.417	0.024	0.008	55.236	0.081	0.022	0	0.057	0.050	100.150
29	41.507	0.040	4.056	0.000	0.004	53.474	0.052	0.005	0	0.089	0.000	97.518

### (2) CATION TOTAL

Grain No.	P	La	F	Si	Cl	Ca	Ce	Na	Sr	Fe	Mn	Total
1	0.2372	0.0001	0.0669	0	0	0.4059	0.0002	0.0003	0	0.0003	0.0001	0.711
2	0.2363	0.0001	0.0615	0.0003	0.0017	0.4049	0.0003	0.0001	0	0.0027	0.0005	0.7085
3	0.2381	0	0.0782	0	0	0.4027	0.0002	0.0001	0	0.0013	0.0004	0.721
4	0.2398	0.0002	0.0703	0	0.0001	0.398	0.0003	0.0001	0	0.0009	0.0007	0.7104
6	0.2379	0.0001	0.0746	0.0002	0.0001	0.4022	0.0005	0.0002	0	0.0011	0.0005	0.7175
7	0.2369	0.0003	0.0719	0	0.0001	0.4054	0.0002	0.0002	0	0.0012	0.0003	0.7165
8	0.2369	0	0.0738	0.0004	0.0002	0.4045	0.0005	0	0	0.0014	0.0002	0.718
9	0.2382	0.0001	0.0785	0	0	0.4034	0.0001	0.0003	0	0.0004	0.0001	0.7212
10	0.2374	0.0002	0.0677	0.0001	0.0006	0.4036	0.0004	0.0001	0	0.0012	0.0004	0.7118
11	0.2388	0	0.0737	0.0004	0.0002	0.3993	0.0005	0	0	0.0017	0.0004	0.7151
12	0.2413	0.0001	0.0731	0.0002	0.0001	0.3949	0.0002	0.0001	0	0.0005	0.0003	0.7109
13	0.24	0.0002	0.0735	0.0003	0.0001	0.3973	0.0001	0.0002	0	0.0011	0.0005	0.7133
14	0.2405	0	0.0783	0.0001	0	0.3977	0.0002	0.0001	0	0.0002	0	0.7171
15	0.2376	0.0003	0.07	0.0003	0.0001	0.4032	0.0003	0.0005	0	0.0009	0.0003	0.7135
16	0.2389	0	0.0914	0.0001	0.0001	0.4012	0.0002	0	0	0.0008	0.0002	0.7329
17	0.2399	0.0002	0.0702	0.0001	0.0001	0.3973	0.0003	0	0	0.0014	0.0005	0.71
18	0.2399	0	0.0733	0.0002	0.0005	0.3959	0.0005	0.0004	0	0.0023	0.0007	0.7138
19	0.2397	0.0003	0.0641	0	0.0001	0.3993	0.0002	0.0004	0	0.0004	0.0002	0.7048
20	0.2397	0.0003	0.0739	0.0003	0.0003	0.3977	0.0002	0.0001	0	0.0012	0.0004	0.7142
21	0.2415	0.0002	0.0644	0	0.0001	0.394	0.0003	0	0	0.0012	0.0004	0.7021
22	0.24	0	0.0723	0.0004	0.0003	0.3964	0.0004	0.0002	0	0.0019	0.0003	0.7122
23	0.2388	0.0003	0.0555	0.0002	0.0008	0.3992	0.0003	0.0001	0	0.0021	0.0003	0.6977
24	0.2384	0	0.0619	0.0003	0.0001	0.4021	0.0003	0.0002	0	0.0007	0.0001	0.7041
25	0.2393	0	0.0779	0	0	0.4005	0.0003	0.0001	0	0.0005	0.0002	0.7189
26	0.2407	0.0001	0.0651	0.0002	0.0001	0.3956	0.0002	0.0001	0	0.0016	0.0002	0.7039
27	0.2398	0.0002	0.086	0.0002	0.0001	0.3988	0.0002	0.0003	0	0.0003	0.0003	0.7262
29	0.2419	0.0001	0.0811	0	0	0.3944	0.0001	0.0001	0	0.0005	0	0.7183

## SAMPLE EOC-14-005

Age: Archean

Rock type: Greywacke

Coordinates

Easting -76.0866

Northing 52.69931

Elevation 220

### GRAIN\_DATA

---

Number of dated grains 12

Sample lab #	Grain#	Ns	Ni	# square	MDpar	MDprp	U (ppm)	Age
<b>NP3</b>	2	24	22	40	N/A	N/A	68	237.3
	3	89	64	50	N/A	N/A	158	301
	7	42	42	30	N/A	N/A	173	217.9
	9	32	17	25	N/A	N/A	84	404.2
	10	35	20	40	N/A	N/A	62	376.6
	12	44	41	100	N/A	N/A	51	233.6
<b>NP19-1</b>	4	66	38	100	2.32	0.70	46	373.9
	5	42	26	60	2.33	0.62	52	348.4
	6	89	58	100	2.28	0.69	69	331.4
	8	74	47	60	2.22	0.67	94	339.8
<b>NP19-2</b>	1	114	65	100	2.49	0.78	78	377.4
	2	30	16	20	2.54	0.85	96	402.7

### LENGTH\_DATA

---

Number\_of\_lens 6

	#	Len	Type	MDpar	MDprp	NDpar	Angle with C-axis
<b>NP19-1 (grain#)</b>							
	8	1	11.666	T	2.426	0.718	4
	8	2	14.061	T	2.426	0.718	4
	8	3	12.538	T	2.426	0.718	4
	8	4	10.93	T	2.426	0.718	4
<b>NP19-2</b>							
	5	1	11.302	T	2.29	0.672	4
	5	2	12.74	T	2.29	0.672	4

## MICROPROBE DATA

---

Mass percent													
	Grain#	P2O5	La2O3	F	SiO2	Cl	CaO	Na2O	SrO	FeO	MnO	Total	
<b>NP3</b>	2	40.135	0.000	2.889	0	0.017	54.142	0.003	0	0.02	0.04	96.04	
	3	40.444	0.105	3.467	0	0.019	54.061	0.000	0	0.00	0.03	96.75	
	7	40.636	0.000	3.423	0	0.013	55.062	0.012	0	0.02	0.00	97.77	
	9	40.113	0.013	2.656	0	0.011	53.963	0.002	0	0.03	0.04	95.75	
	10	39.673	0.004	3.002	0	0.011	54.765	0.000	0	0.06	0.00	96.29	
	12	39.918	0.086	3.176	0	0.006	54.791	0.011	0	0.00	0.01	96.72	
<b>NP19-1</b>	4	40.429	0.088	3.801	0	0.019	54.679	0.009	0	0.05	0.02	97.52	
	5	40.562	0.000	3.694	0	0.010	55.020	0.011	0	0.03	0.02	97.79	
	6	40.715	0.000	3.427	0	0.013	54.917	0.010	0	0.03	0.07	97.76	
	8	40.516	0.011	3.229	0	0.014	54.735	0.022	0	0.03	0.06	97.25	
<b>NP19-2</b>	1	40.277	0.000	3.318	0	0.008	55.103	0.017	0	0.00	0.03	97.35	
	2	39.729	0.009	3.597	0	0.014	54.088	0.022	0	0.03	0.03	96.07	
Cation total													
	Grain#	P	La	F	Si	Cl	Ca	Ce	Na	Sr	Fe	Mn	Total
<b>NP3</b>	2	0.2376	0	0.06	0	0.0002	0.4056	0.0001	0	0	0.0001	0.0002	0.7039
	3	0.2384	0.0003	0.0709	0	0.0002	0.4032	0.0002	0	0	0	0.0002	0.7134
	7	0.2372	0	0.0694	0	0.0001	0.4067	0.0001	0.0002	0	0.0001	0	0.7139
	9	0.2378	0	0.0555	0	0.0001	0.4049	0.0001	0	0	0.0002	0.0002	0.6988
	10	0.2353	0	0.0624	0	0.0001	0.4111	0.0001	0	0	0.0003	0	0.7093
	12	0.2359	0.0002	0.0655	0	0.0001	0.4097	0.0001	0.0002	0	0	0.0001	0.7119
<b>NP19-1</b>	4	0.2372	0.0002	0.0769	0	0.0002	0.406	0.0001	0.0001	0	0.0003	0.0001	0.7212
	5	0.2371	0	0.0746	0	0.0001	0.407	0	0.0001	0	0.0002	0.0001	0.7193
	6	0.2375	0	0.0695	0	0.0001	0.4054	0.0001	0.0001	0	0.0002	0.0004	0.7133
	8	0.2374	0	0.066	0	0.0002	0.4058	0	0.0003	0	0.0002	0.0004	0.7103
<b>NP19-2</b>	1	0.2363	0	0.0678	0	0.0001	0.4091	0	0.0002	0	0	0.0001	0.7136
	2	0.2366	0	0.0741	0	0.0002	0.4077	0.0002	0.0003	0	0.0002	0.0002	0.7195

## SAMPLE EUG-15-018A

Age: Archean  
 Rock type: Greywacke

Coordinates

Easting -76.08679  
 Northing 52.70057  
 Elevation -5

**GRAIN\_DATA**

Number of dated grains 12								
Sample lab #	Grain#	Ns	Ni	#square	MDpar	MDprp	U (ppm)	AFT age
<b>NP15</b>	1	41	21	10	2.08	0.73	256	425.9
	2	46	26	10	2.48	0.78	316	387.1
	3	29	18	10	2.43	0.81	219	353.5
	5	42	19	10	2.39	0.67	231	480.2
	7	42	26	10	2.49	0.70	316	354.4
<b>NP20-2</b>	1	49	23	15	2.45	0.68	181	463.4
	3	72	48	10	2.71	0.84	566	329.7
	11	44	14	10	2.33	0.66	165	672.4
	12	35	17	16	2.29	0.72	125	448.3
	14	50	33	16	2.36	0.68	243	332.9
	16	38	31	16	2.45	0.61	228	270.7
	18	39	17	12	2.32	0.78	167	497.6

**LENGTH\_DATA**

Number_of_Lens 128						
#	Len	Type	MDpar	MDprp	NDpar	Angle with C-axis
IP15 (grain#)						
1	1	11.48	T	2.56	0.86	4
1	2	8.87	T	2.56	0.86	4
1	3	13.78	T	2.56	0.86	4
1	4	13.68	T	2.56	0.86	4
1	5	14.30	T	2.56	0.86	4
1	6	14.69	T	2.56	0.86	4
1	7	14.90	T	2.56	0.86	4
1	8	10.87	T	2.56	0.86	4
1	9	9.00	T	2.56	0.86	4
1	10	11.71	T	2.56	0.86	4
1	11	10.47	T	2.56	0.86	4
1	12	13.41	T	2.56	0.86	4
1	13	11.35	T	2.56	0.86	4
1	14	13.94	T	2.56	0.86	4
2	15	13.90	T	2.49	0.69	4
2	16	9.63	T	2.49	0.69	4
2	17	10.34	T	2.49	0.69	4
2	18	12.28	T	2.49	0.69	4
2	19	12.72	T	2.49	0.69	4
2	20	13.48	T	2.49	0.69	4
2	21	14.52	T	2.49	0.69	4
2	22	13.24	T	2.49	0.69	4
2	23	12.80	T	2.49	0.69	4
2	24	9.02	T	2.49	0.69	4
2	25	13.77	T	2.49	0.69	4
2	26	13.78	T	2.49	0.69	4
2	27	12.99	T	2.49	0.69	4
2	28	13.66	T	2.49	0.69	4
2	29	14.10	T	2.49	0.69	4
2	30	13.99	T	2.49	0.69	4
3	31	6.76	T	2.17	0.72	4
3	32	10.12	T	2.17	0.72	4
3	33	12.07	T	2.17	0.72	4
3	34	10.66	T	2.17	0.72	4
3	35	11.83	T	2.17	0.72	4
3	36	10.63	T	2.17	0.72	4
3	37	13.31	T	2.17	0.72	4
3	38	12.74	T	2.17	0.72	4
3	39	11.11	T	2.17	0.72	4
3	40	12.44	T	2.17	0.72	4
3	41	12.10	T	2.17	0.72	4
3	42	11.17	T	2.17	0.72	4
3	43	10.77	T	2.17	0.72	4
3	44	15.20	T	2.17	0.72	4
3	45	14.30	T	2.17	0.72	4
5	46	13.38	T	2.20	0.57	4
5	47	10.51	T	2.20	0.57	4
5	48	12.54	T	2.20	0.57	4

5	49	12.23	T	2.20	0.57	4	85.14
5	50	13.17	T	2.20	0.57	4	78.70
5	51	7.98	T	2.20	0.57	4	63.60
5	52	12.64	T	2.20	0.57	4	63.93
5	53	12.74	T	2.20	0.57	4	48.05
5	54	11.04	T	2.20	0.57	4	44.97
5	55	7.72	T	2.20	0.57	4	70.51
5	56	14.24	T	2.20	0.57	4	61.11
5	57	14.13	T	2.20	0.57	4	82.18
5	58	13.04	T	2.20	0.57	4	65.27
5	59	12.65	T	2.20	0.57	4	77.02
5	60	15.48	T	2.20	0.57	4	53.01
5	61	11.76	T	2.20	0.57	4	54.82
5	62	15.21	T	2.20	0.57	4	72.48
5	63	13.26	T	2.20	0.57	4	75.34
5	64	14.54	T	2.20	0.57	4	48.78
5	65	12.04	T	2.20	0.57	4	66.63
5	66	9.55	T	2.20	0.57	4	88.14
5	67	10.85	T	2.20	0.57	4	82.25
5	68	10.43	T	2.20	0.57	4	71.16
5	69	12.20	T	2.20	0.57	4	45.56
5	70	12.77	T	2.20	0.57	4	69.68
5	71	13.83	T	2.20	0.57	4	61.04
5	72	8.84	T	2.20	0.57	4	71.73
6	73	15.36	T	2.40	0.85	4	75.87
6	74	11.62	T	2.40	0.85	4	50.71
6	75	12.82	T	2.40	0.85	4	85.84
6	76	14.97	T	2.40	0.85	4	84.26
6	77	14.14	T	2.40	0.85	4	39.32
6	78	15.73	T	2.40	0.85	4	29.33
6	79	12.54	T	2.40	0.85	4	53.61
6	80	12.75	T	2.40	0.85	4	62.25
6	81	10.17	T	2.40	0.85	4	71.86
6	82	11.14	T	2.40	0.85	4	71.57
6	83	13.46	T	2.40	0.85	4	75.97
6	84	13.07	T	2.40	0.85	4	58.35
6	85	10.73	T	2.40	0.85	4	47.96
6	86	13.70	T	2.40	0.85	4	70.17
6	87	14.80	T	2.40	0.85	4	75.14
6	88	11.34	T	2.40	0.85	4	82.40
6	89	12.88	T	2.40	0.85	4	69.73
7	90	11.70	T	2.42	0.78	4	56.14
7	91	13.33	T	2.42	0.78	4	63.07
7	92	12.31	T	2.42	0.78	4	72.51
7	93	9.10	T	2.42	0.78	4	83.30
7	94	14.18	T	2.42	0.78	4	81.51
7	95	12.26	T	2.42	0.78	4	77.16
7	96	14.14	T	2.42	0.78	4	79.65
7	97	14.26	T	2.42	0.78	4	63.74
7	98	14.24	T	2.42	0.78	4	59.83
7	99	12.93	T	2.42	0.78	4	49.85
7	100	12.10	T	2.42	0.78	4	78.33
7	101	13.67	T	2.42	0.78	4	80.98
7	102	12.49	T	2.42	0.78	4	76.30
7	103	12.45	T	2.42	0.78	4	78.12
7	104	9.98	T	2.42	0.78	4	76.45
1	1	13.68	T	2.42	0.71	4	42.745
1	2	11.22	T	2.42	0.71	4	62.076
1	3	14.73	T	2.42	0.71	4	75.069
3	4	14.87	T	2.37	0.80	4	77.24
3	5	13.51	T	2.37	0.80	4	88.914
3	6	9.97	T	2.37	0.80	4	56.594
3	7	13.14	T	2.37	0.80	4	68.645
3	8	12.67	T	2.37	0.80	4	59.398
3	9	7.67	T	2.37	0.80	4	66.645
3	10	11.45	T	2.37	0.80	4	51.853
3	11	11.43	T	2.37	0.80	4	37.098
11	12	16.10	T	2.32	0.69	4	46.012
11	13	13.90	T	2.32	0.69	4	66.098
11	14	13.46	T	2.32	0.69	4	84.828
12	15	11.11	T	2.38	0.68	4	73.101
12	16	12.41	T	2.38	0.68	4	58.277
12	17	14.19	T	2.38	0.68	4	41.954
12	18	14.10	T	2.38	0.68	4	89.177
14	19	10.09	T	2.41	0.72	4	38.662
14	20	13.99	T	2.41	0.72	4	79.511
16	21	14.83	T	2.07	0.70	4	50.705
16	22	13.34	T	2.07	0.70	4	83.324
16	23	12.65	T	2.07	0.70	4	65.07
16	24	12.93	T	2.07	0.70	4	64.461

## MICROPROBE DATA

---

### Mass percent

		P2O5	La2O3	F	SiO2	Cl	CaO	Na2O	SrO	FeO	MnO	Total
<b>NP15</b>	1	40.808	0.000	3.390	0	0.004	54.458	0.000	0	0.000	0.062	97.365
	2	41.020	0.000	3.914	0	0.005	54.349	0.003	0	0.018	0.025	97.725
	3	40.496	0.000	3.704	0	0.003	55.035	0.007	0	0.000	0.020	97.762
	5	40.909	0.014	3.484	0	0.000	54.288	0.000	0	0.039	0.057	97.361
	7	40.649	0.057	3.170	0	0.000	54.539	0.003	0	0.026	0.000	97.159
<b>NP20-2</b>	1	40.504	0.003	3.494	0	0.000	55.051	0.001	0	0.017	0.000	97.628
	3	40.183	0.157	3.632	0	0.000	54.687	0.000	0	0.038	0.012	97.249
	11	40.966	0.064	3.621	0	0.001	55.481	0.008	0	0.000	0.027	98.706
	12	40.814	0.000	3.634	0	0.000	54.931	0.025	0	0.000	0.000	97.906
	14	40.616	0.000	3.202	0	0.000	55.053	0.015	0	0.038	0.005	97.686
	16	40.753	0.078	3.522	0	0.000	54.960	0.000	0	0.027	0.027	98.037
	18	41.177	0.000	3.224	0	0.008	55.198	0.013	0	0.000	0.000	98.351

		P	La	F	Si	Cl	Ca	Ce	Na	Sr	Fe	Mn	Total
<b>NP15</b>	1	0.2386	0	0.0689	0	0	0.4029	0.0002	0	0	0	0.0004	0.711
	2	0.2393	0	0.0786	0	0	0.4013	0.0001	0	0	0.0001	0.0001	0.7196
	3	0.2369	0	0.0749	0	0	0.4074	0.0001	0.0001	0	0	0.0001	0.7196
	5	0.2391	0	0.0707	0	0	0.4015	0.0001	0	0	0.0002	0.0003	0.712
	7	0.2381	0.0001	0.0648	0	0	0.4042	0.0001	0	0	0.0002	0	0.7075
<b>NP20-2</b>	1	0.2369	0	0.0709	0	0	0.4075	0.0001	0	0	0.0001	0	0.7156
	3	0.2366	0.0004	0.074	0	0	0.4074	0.0002	0	0	0.0002	0.0001	0.7189
	11	0.2371	0.0002	0.0726	0	0	0.4064	0.0002	0.0001	0	0	0.0002	0.7168
	12	0.2378	0	0.0733	0	0	0.4051	0.0001	0.0003	0	0	0	0.7167
	14	0.2371	0	0.0652	0	0	0.4066	0.0003	0.0002	0	0.0002	0	0.7096
	16	0.2374	0.0002	0.0712	0	0	0.4052	0.0004	0	0	0.0002	0.0002	0.7148
	18	0.2382	0	0.0651	0	0.0001	0.4041	0.0002	0.0002	0	0	0	0.7079

## SAMPLE EUG-14-20C

Age: Archean

Rock type: Greywackes

Coordinates

Easting -76.08623

Northing 52.70091

Elevation -162

### **GRAIN\_DATA**

Number of dated grain 24

Sample lat	Grain#	Ns	Ni	# square	MDpar	MDprp	U (ppm)
<b>NP2</b>	1	7	8	8	2.946	0.613	124
	2	16	10	10	2.643	0.7	124
	3	24	12	25	2.248	0.555	60
	6	14	15	21	2.383	0.714	89
	7	17	9	16	2.369	0.634	70
	8	21	13	30	2.426	0.69	54
	9	27	12	21	2.184	0.586	71
	11	41	20	40	2.183	0.562	62
	12	30	22	40	2.404	0.612	68
	13	22	15	25	2.352	0.719	75
	15	5	8	25	2.233	0.534	40
	16	112	73	49	2.196	0.525	185
	<b>NP18-1</b>	2	8	5	12	2.173	0.537
		4	11	11	28	2.103	0.63
		5	31	13	40	2.177	0.701
		8	8	7	10	2.163	0.73
		11	13	10	24	1.943	0.57
		14	18	7	25	1.939	0.536
		15	5	8	32	2.029	0.437
		16	8	12	20	2.371	0.641
		17	13	18	30	2.033	0.585
<b>NP18-2</b>	2	8	6	16	2.401	0.747	45
	4	56	29	70	2.569	0.879	50
	7	35	23	30	2.27	0.616	93

### **LENGTH\_DATA**

Number\_of\_lens 24

	#	Len	Type	MDpar	MDprp	NDpar	Angle with
<b>NP2 (grain#)</b>							
6	1	8.636	T	2.222	0.585	4	49.501
6	2	14.301	T	2.222	0.585	4	69.313
6	3	14.817	T	2.222	0.585	4	32.698
6	4	17.842	T	2.222	0.585	4	83.123
7	5	6.885	T	2.213	0.65	4	84.87
8	6	9.7	T	2.37	0.614	4	35.148
8	7	13.181	T	2.37	0.614	4	14.01
9	8	14.087	T	2.263	0.606	4	55.405
9	9	7.535	T	2.263	0.606	4	57.059
9	10	13.779	T	2.263	0.606	4	33.563
12	11	9.593	T	2.329	0.6	4	47.77
12	12	12.133	T	2.329	0.6	4	62.061
13	13	12.341	T	2.316	0.611	4	87.131
13	14	10.991	T	2.316	0.611	4	61.86
16	15	10.119	T	2.361	0.626	4	30.626
16	16	10.764	T	2.361	0.626	4	40.45
16	17	9.84	T	2.361	0.626	4	43.509
16	18	13.062	T	2.361	0.626	4	83.602
16	19	13.616	T	2.361	0.626	4	73.209
16	20	12.797	T	2.361	0.626	4	24.958
16	21	9.487	T	2.361	0.626	4	48.304
16	22	13.463	T	2.361	0.626	4	65.864
<b>NP18-1</b>							
2	1	13.014	T	2.231	0.625	4	45.224
4	2	14.126	T	1.968	0.65	4	71.232

---

**MICROPROBE DATA**


---

**Mass percent**

	Grain#	P2O5	La2O3	F	SiO2	Cl	CaO	Ce2O3	Na2O	SrO	FeO	MnO	Total
<b>NP2</b>	1	39.999	0.008	3.596	0	0.000	54.170	0.000	0.059	0	0.049	0.171	96.538
	2	40.912	0.079	3.816	0	0.008	54.469	0.071	0.053	0	0.016	0.154	97.969
	3	40.511	0.007	3.573	0	0.006	54.531	0.029	0.028	0	0.026	0.128	97.334
	6	40.995	0.043	3.678	0	0.005	54.624	0.061	0.007	0	0.000	0.161	98.024
	7	40.652	0.000	3.835	0	0.004	54.485	0.000	0.012	0	0.015	0.079	97.466
	8	40.858	0.000	3.855	0	0.000	54.765	0.016	0.037	0	0.003	0.135	98.046
	9	40.748	0.050	3.939	0	0.000	54.563	0.082	0.038	0	0.072	0.150	97.983
	11	40.620	0.000	3.408	0	0.004	54.358	0.108	0.033	0	0.002	0.165	97.262
	12	40.594	0.002	3.618	0	0.000	54.672	0.077	0.060	0	0.041	0.162	97.703
	13	41.441	0.000	3.624	0	0.004	54.281	0.034	0.058	0	0.000	0.128	98.043
	15	40.736	0.000	3.173	0	0.005	54.651	0.048	0.030	0	0.047	0.128	97.481
	16	40.675	0.024	3.902	0	0.002	54.388	0.050	0.041	0	0.014	0.112	97.565
<b>NP18-1</b>	2	40.167	0.060	3.905	0	0.002	53.951	0.000	0.045	0	0.024	0.156	96.666
	4	40.093	0.018	3.574	0	0.007	54.242	0.005	0.047	0	0.002	0.181	96.662
	5	41.044	0.037	3.968	0	0.005	54.426	0.000	0.050	0	0.069	0.131	98.058
	8	40.249	0.024	3.870	0	0.000	54.490	0.040	0.037	0	0.019	0.145	97.245
	11	40.824	0.000	3.662	0	0.007	54.465	0.040	0.053	0	0.033	0.140	97.680
	14	40.707	0.032	3.479	0	0.000	54.139	0.055	0.046	0	0.000	0.163	97.156
	15	40.260	0.000	3.943	0	0.004	54.317	0.069	0.020	0	0.029	0.097	97.078
	16	40.928	0.000	3.450	0	0.000	54.333	0.050	0.045	0	0.000	0.128	97.481
	17	40.325	0.000	3.865	0	0.000	54.462	0.000	0.038	0	0.014	0.094	97.171
<b>NP18-2</b>	2	40.390	0.000	3.726	0	0.000	54.841	0.055	0.031	0	0.085	0.146	97.705
	4	40.724	0.000	3.767	0	0.000	54.648	0.069	0.059	0	0.006	0.141	97.828
	7	41.142	0.000	3.328	0	0.006	54.793	0.095	0.048	0	0.000	0.157	98.167

**Cation total**

	Grain#	P	La	F	Si	Cl	Ca	Ce	Na	Sr	Fe	Mn	Total
<b>NP2</b>	1	0.2369	0	0.0737	0	0	0.406	0	8E-04	0	0.0003	0.001	0.7188
	2	0.2385	0.0002	0.0767	0	0.0001	0.4018	0.0002	7E-04	0	0.0001	0.0009	0.7192
	3	0.2376	0	0.0726	0	0.0001	0.4048	0.0001	4E-04	0	0.0002	0.0008	0.7167
	6	0.2385	0.0001	0.074	0	0.0001	0.4023	0.0002	1E-04	0	0	0.0009	0.7163
	7	0.2382	0	0.0774	0	0	0.404	0	2E-04	0	0.0001	0.0005	0.7204
	8	0.238	0	0.0774	0	0	0.4038	0	5E-04	0	0	0.0008	0.7206
	9	0.2379	0.0001	0.0791	0	0	0.4032	0.0002	5E-04	0	0.0004	0.0009	0.7223
	11	0.2381	0	0.0694	0	0	0.4032	0.0003	4E-04	0	0	0.001	0.7125
	12	0.2374	0	0.0732	0	0	0.4046	0.0002	8E-04	0	0.0002	0.001	0.7174
	13	0.2402	0	0.0727	0	0	0.3982	0.0001	8E-04	0	0	0.0007	0.7128
	15	0.2379	0	0.0647	0	0.0001	0.4039	0.0001	4E-04	0	0.0003	0.0007	0.7081
	16	0.2382	0.0001	0.0786	0	0	0.4031	0.0001	6E-04	0	0.0001	0.0007	0.7216
<b>NP18-1</b>	2	0.2377	0.0002	0.0795	0	0	0.4041	0	6E-04	0	0.0001	0.0009	0.7232
	4	0.2371	0	0.0732	0	0.0001	0.4059	0	6E-04	0	0	0.0011	0.7181
	5	0.239	0.0001	0.0794	0	0.0001	0.401	0	7E-04	0	0.0004	0.0008	0.7215
	8	0.237	0.0001	0.0784	0	0	0.406	0.0001	5E-04	0	0.0001	0.0009	0.7232
	11	0.2384	0	0.074	0	0.0001	0.4025	0.0001	7E-04	0	0.0002	0.0008	0.7168
	14	0.2387	0.0001	0.0708	0	0	0.4017	0.0001	6E-04	0	0	0.001	0.7131
	15	0.2374	0	0.0799	0	0	0.4053	0.0002	3E-04	0	0.0002	0.0006	0.7239
	16	0.2389	0	0.07	0	0	0.4014	0.0001	6E-04	0	0	0.0008	0.7118
	17	0.2374	0	0.0783	0	0	0.4057	0	5E-04	0	0.0001	0.0006	0.7227
<b>NP18-2</b>	2	0.2366	0	0.0754	0	0	0.4066	0.0001	4E-04	0	0.0005	0.0009	0.7206
	4	0.2378	0	0.0759	0	0	0.4039	0.0002	8E-04	0	0	0.0008	0.7194
	7	0.2385	0	0.0672	0	0.0001	0.402	0.0002	6E-04	0	0	0.0009	0.7095

## SAMPLE MKB-12-493

Age: Archean

Rock type: banded iron formation

Coordinates

Easting -96.07229

Northing 65.02244

Elevation 140 (approximative)

### **GRAIN\_DATA**

Number of dated grains 29

Sample lab #	Grain#	Ns	Ni	# square	MDpar	MDprp	U (ppm)
<b>NP14</b>	2	60	25	100	2.52	0.67	31
	4	43	21	100	2.27	0.65	26
	5	33	23	100	2.19	0.82	28
	6	19	10	50	2.50	0.76	24
	8	27	11	50	2.49	0.71	27
	11	23	12	60	2.39	0.62	24
	14	60	29	100	2.40	0.82	35
	15	39	15	100	2.55	0.82	18
	16	22	13	60	2.34	0.77	27
	17	31	19	100	2.21	0.77	23
	18	29	19	100	2.26	0.80	23
	20	22	8	50	2.30	0.62	20
	21	38	24	100	2.21	0.58	29
<b>NP21-2</b>	2	52	29	100	2.29	0.83	34
	3	45	17	70	2.56	0.84	28
	4	43	16	80	2.57	1.00	23
	5	35	25	70	2.55	1.00	42
	11	47	23	100	2.36	0.77	27
	12	24	12	60	2.45	0.83	23
	14	64	27	100	2.35	0.80	32
	15	42	18	100	2.52	0.64	21
	17	46	23	100	2.46	0.69	27
	21	45	21	90	2.27	0.65	27
	24	32	14	50	2.80	0.72	33
	27	69	28	100	2.49	0.78	33
	28	58	24	100	2.59	0.82	28
	30	41	22	100	2.60	0.81	26
	31	50	24	100	2.27	0.83	28
	32	46	26	100	2.34	0.88	30

## LENGTH\_DATA

Number_of_lens	32	#	Len	Type	MDpar	MDpr	NDpar	Angle with C-axis
<b>IP14 (grain#)</b>								
2	1	12.249	T	2.49	0.767	4	87.581	
2	2	13.289	T	2.49	0.767	4	83.368	
2	3	11.081	T	2.49	0.767	4	72.85	
2	4	11.015	T	2.49	0.767	4	80.734	
4	5	13.714	T	2.43	0.736	4	57.974	
4	6	9.292	T	2.43	0.736	4	69.474	
4	7	9.938	T	2.43	0.736	4	53.641	
5	8	10.058	T	2.241	0.604	4	67.852	
5	9	11.959	T	2.241	0.604	4	82.933	
6	10	11.484	T	2.309	0.848	4	56.668	
8	11	11.221	T	2.377	0.746	4	54.272	
8	12	15.182	T	2.377	0.746	4	7.21	
11	13	14.424	T	2.43	0.754	4	60.085	
14	14	14.22	T	2.36	0.67	4	74.512	
17	15	11.087	T	2.303	0.699	4	35.965	
17	16	13.303	T	2.303	0.699	4	39.212	
21	17	10.311	T	2.064	0.611	4	67.276	
21	18	12.461	T	2.064	0.611	4	89.077	
<b>NP21-2</b>								
3	1	11.96	T	2.609	0.796	4	55.473	
3	2	10.914	T	2.609	0.796	4	65.298	
3	3	14.426	T	2.609	0.796	4	67.851	
3	4	10.549	T	2.609	0.796	4	52.742	
3	5	15.331	T	2.609	0.796	4	68.196	
3	6	13.144	T	2.609	0.796	4	69.743	
11	7	12.927	T	2.374	0.711	4	61.884	
17	8	10.88	T	2.544	0.888	4	57.721	
27	9	13.896	T	2.599	0.863	4	77.38	
27	10	13.433	T	2.599	0.863	4	39.166	
28	11	10.988	T	2.368	0.874	4	34.115	
28	12	11.032	T	2.368	0.874	4	50.546	
28	13	12.794	T	2.368	0.874	4	78.364	
32	14	14.02	T	2.52	0.761	4	83.337	

## MICROPROBE DATA

Mass percent												
	P2O5	La2O3	F	SiO2	Cl	CaO	Ce2O3	Na2O	SrO	FeO	MnO	Total
<b>NP14</b>	2	40.481	0.000	2.850	0	0.06	54.76	0.05	0.01	0	0.00	0.02
	4	40.899	0.052	2.985	0	0.06	55.65	0.00	0.02	0	0.01	0.01
	5	41.351	0.006	3.395	0	0.07	55.53	0.00	0.01	0	0.06	0.03
	6	41.193	0.036	3.110	0	0.06	55.19	0.03	0.03	0	0.04	0.03
	8	41.677	0.029	3.396	0	0.06	54.96	0.01	0.01	0	0.02	0.04
	11	41.543	0.000	3.073	0	0.06	54.99	0.00	0.03	0	0.01	0.07
	14	41.267	0.000	2.888	0	0.05	54.73	0.03	0.00	0	0.01	0.04
	15	40.944	0.000	3.204	0	0.07	54.91	0.06	0.01	0	0.00	0.01
	16	40.623	0.052	3.583	0	0.08	55.02	0.00	0.02	0	0.03	0.00
	17	41.111	0.000	3.004	0	0.06	55.15	0.00	0.03	0	0.00	0.04
	18	41.302	0.000	2.987	0	0.06	55.36	0.03	0.01	0	0.00	0.04
	20	40.989	0.018	2.658	0	0.04	55.03	0.01	0.01	0	0.01	0.01
	21	41.041	0.043	3.060	0	0.04	54.55	0.02	0.00	0	0.01	0.02
<b>NP21-2</b>	2	41.057	0.000	2.753	0	0.07	54.78	0.01	0.06	0	0.00	0.04
	3	40.924	0.000	2.760	0	0.04	54.65	0.03	0.00	0	0.00	0.01
	4	41.006	0.000	3.178	0	0.05	55.05	0.04	0.03	0	0.04	0.05
	5	40.646	0.000	3.135	0	0.09	54.96	0.02	0.03	0	0.02	0.00
	11	40.778	0.000	3.340	0	0.06	55.22	0.00	0.01	0	0.05	0.00
	12	41.105	0.098	3.419	0	0.05	54.92	0.07	0.02	0	0.00	0.00
	14	41.470	0.000	3.015	0	0.06	54.94	0.00	0.04	0	0.05	0.03
	15	40.770	0.068	2.870	0	0.04	55.40	0.01	0.02	0	0.03	0.04
	17	40.708	0.029	3.005	0	0.08	54.92	0.00	0.00	0	0.00	0.02
	21	40.952	0.000	3.208	0	0.08	54.92	0.00	0.00	0	0.01	0.04
	24	40.999	0.000	3.006	0	0.07	55.43	0.06	0.02	0	0.01	0.01
	27	41.080	0.079	3.150	0	0.08	54.93	0.12	0.02	0	0.00	0.05
	28	41.126	0.022	3.085	0	0.05	55.58	0.00	0.02	0	0.03	0.05
	30	40.649	0.086	2.773	0	0.05	54.75	0.04	0.01	0	0.00	0.00
	31	41.315	0.061	3.049	0	0.07	55.09	0.03	0.02	0	0.02	0.06
	32	41.529	0.000	2.771	0	0.09	54.52	0.07	0.00	0	0.00	0.05

	P	La	F	Si	Cl	Ca	Ce	Na	Sr	Fe	Mn	Total
<b>NP14</b>	2	0.2373	0	0.0587	0	0.0007	0.4063	0.0001	0.0002	0	0	0.0001
	4	0.2368	0.0001	0.0606	0	0.0006	0.4076	0	0.0003	0	1E-04	0.0001
	5	0.238	0	0.068	0	0.0007	0.4044	0	0.0002	0	3E-04	0.0001
	6	0.2382	0.0001	0.0629	0	0.0007	0.4038	0.0001	0.0004	0	2E-04	0.0002
	8	0.2397	0.0001	0.068	0	0.0006	0.4001	0	0.0002	0	1E-04	0.0002
	11	0.2394	0	0.062	0	0.0006	0.401	0	0.0004	0	1E-04	0.0004
	14	0.2392	0	0.0588	0	0.0006	0.4015	0.0001	0	0	0	0.0002
	15	0.2382	0	0.065	0	0.0007	0.4042	0.0002	0.0001	0	0	0.0001
	16	0.2372	0.0001	0.0724	0	0.0009	0.4066	0	0.0002	0	2E-04	0
	17	0.2381	0	0.061	0	0.0006	0.4043	0	0.0004	0	0	0.0002
	18	0.2382	0	0.0604	0	0.0007	0.4041	0.0001	0.0001	0	0	0.0002
	20	0.2381	0	0.0545	0	0.0004	0.4045	0	0.0001	0	0	0.0001
	21	0.239	0.0001	0.0624	0	0.0004	0.4021	0.0001	0	0	1E-04	0.0001
<b>NP21-2</b>	2	0.2386	0	0.0563	0	0.0008	0.4029	0	0.0007	0	0	0.0002
	3	0.2386	0	0.0567	0	0.0004	0.4032	0.0001	0	0	0	0.0001
	4	0.238	0	0.0644	0	0.0005	0.4043	0.0001	0.0004	0	2E-04	0.0003
	5	0.2374	0	0.064	0	0.0009	0.4062	0	0.0005	0	1E-04	0
	11	0.2372	0	0.0676	0	0.0007	0.4066	0	0.0001	0	3E-04	0
	12	0.2384	0.0002	0.0689	0	0.0006	0.4032	0.0002	0.0003	0	0	0.0002
	14	0.2393	0	0.061	0	0.0007	0.4011	0	0.0005	0	3E-04	0.0002
	15	0.2368	0.0002	0.0586	0	0.0005	0.4072	0	0.0003	0	2E-04	0.0002
	17	0.2376	0.0001	0.0614	0	0.0009	0.4057	0	0	0	0	0.0001
	21	0.2382	0	0.0651	0	0.0008	0.4043	0	0	0	0	0.0002
	24	0.2374	0	0.061	0	0.0008	0.4061	0.0001	0.0003	0	1E-04	0.0001
	27	0.2383	0.0002	0.0638	0	0.0009	0.4032	0.0003	0.0002	0	0	0.0003
	28	0.2374	0.0001	0.0623	0	0.0006	0.406	0	0.0003	0	1E-04	0.0003
	30	0.2377	0.0002	0.0571	0	0.0006	0.4052	0.0001	0.0001	0	0	0.7011
	31	0.2386	0.0002	0.0617	0	0.0008	0.4026	0.0001	0.0003	0	1E-04	0.0003
	32	0.2402	0	0.0564	0	0.001	0.399	0.0002	0	0	0	0.0003